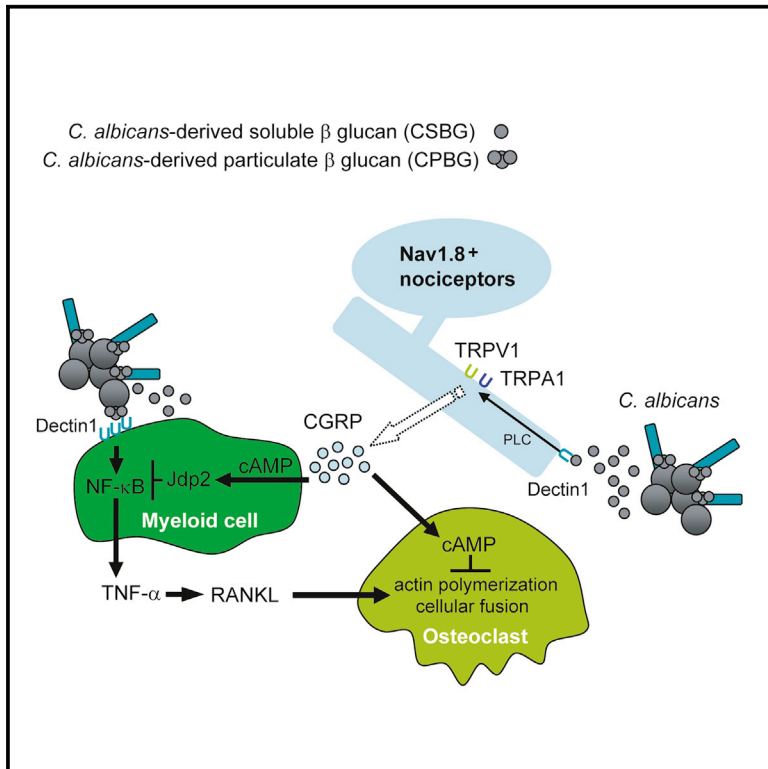


Cell Reports

Nociceptors Boost the Resolution of Fungal Osteoinflammation via the TRP Channel-CGRP-Jdp2 Axis

Graphical Abstract



Authors

Kenta Maruyama, Yasunori Takayama, Takeshi Kondo, ..., Naoki Takemura, Makoto Tominaga, Shizuo Akira

Correspondence

maruyama@biken.osaka-u.ac.jp

In Brief

Maruyama et al. find that Nav1.8-positive nociceptors function during in fungal inflammation.

Highlights

- Fungi activate neurons via the Dectin-1-TRP channel axis, leading to CGRP production
- Nav1.8-positive neurons inhibit osteoporosis and osteomyelitis in response to β -glucan
- TRPV1/TRPA1 deficiency exhibits severe osteoinflammation in response to β -glucan
- Nociceptor-derived CGRP inhibits β -glucan-induced NF- κ B activation via Jdp2



Nociceptors Boost the Resolution of Fungal Osteoinflammation via the TRP Channel-CGRP-Jdp2 Axis

Kenta Maruyama,^{1,8,9,*} Yasunori Takayama,^{2,3,8} Takeshi Kondo,¹ Ken-ichi Ishibashi,⁴ Bikash Ranjan Sahoo,¹ Hisashi Kanemaru,¹ Yutaro Kumagai,¹ Mikaël M. Martino,^{1,5} Hiroki Tanaka,¹ Naohito Ohno,⁴ Yoichiro Iwakura,⁶ Naoki Takemura,⁷ Makoto Tominaga,^{2,3} and Shizuo Akira¹

¹Laboratory of Host Defense, WPI Immunology Frontier Research Center (IFReC), Osaka University, Osaka 565-0871, Japan

²Division of Cell Signaling, Okazaki Institute for Integrative Bioscience, National Institute for Physiological Sciences, National Institutes of Natural Sciences, Aichi 444-8787, Japan

³Department of Physiological Sciences, the Graduate University for Advanced Studies, Aichi 444-8787, Japan

⁴Laboratory for Immunopharmacology of Microbial Products, School of Pharmacy, Tokyo University of Pharmacy and Life Sciences, 1432-1 Horinouchi, Hachioji, Tokyo 192-0392, Japan

⁵European Molecular Biology Laboratory Australia, Australian Regenerative Medicine Institute, Monash University, Melbourne, VIC 3800, Australia

⁶Research Institute for Biomedical Sciences, Tokyo University of Science, 2669 Yamazaki, Noda, Chiba 278-0022, Japan

⁷Department of Mucosal Immunology, School of Medicine, Chiba University, Chiba 260-8670, Japan

⁸These authors contributed equally

⁹Lead Contact

*Correspondence: maruyama@biken.osaka-u.ac.jp
<http://dx.doi.org/10.1016/j.celrep.2017.06.002>

SUMMARY

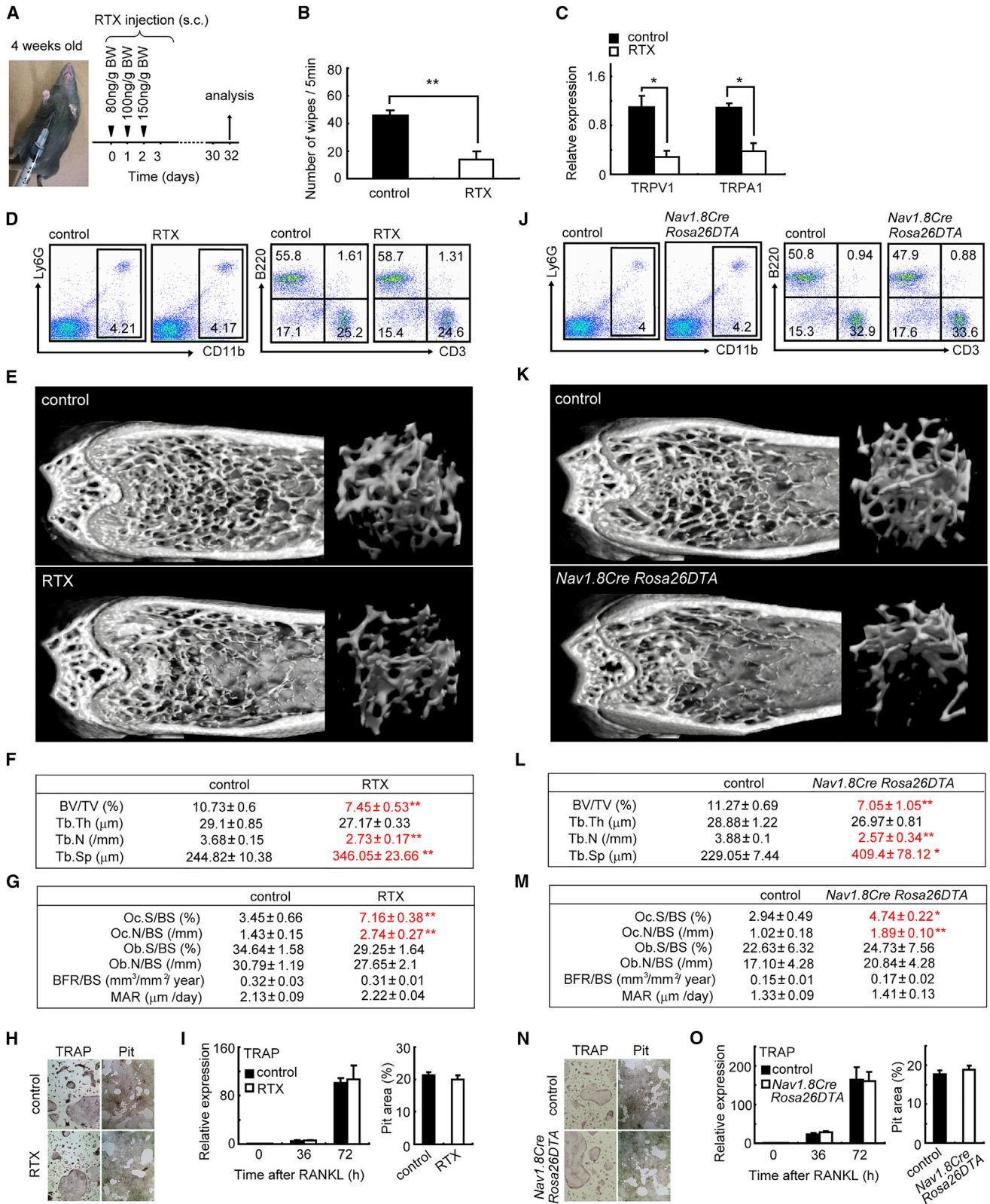
Candida albicans can enter skeletal tissue through a skin wound in an immunocompromised host or by contamination during orthopedic surgery. Such *Candida* osteomyelitis is accompanied by severe pain and bone destruction. It is established that nociceptor innervation occurs in skin and bone, but the mechanisms of nociceptive modulation in fungal inflammation remain unclear. In this study, we show that *C. albicans* stimulates Nav1.8-positive nociceptors via the β -glucan receptor Dectin-1 to induce calcitonin gene-related peptide (CGRP). This induction of CGRP is independent of Bcl-10 or Malt-1 but dependent on transient receptor potential cation channel subfamily V member 1 (TRPV1)/transient receptor potential cation channel subfamily A member 1 (TRPA1) ion channels. Hind-paw β -glucan injection after Nav1.8-positive nociceptor ablation or in TRPV1/TRPA1 deficiency showed dramatically increased osteoinflammation accompanied by impaired CGRP production. Strikingly, CGRP suppressed β -glucan-induced inflammation and osteoclast multinucleation via direct suppression of nuclear factor- κ B (NF- κ B) p65 by the transcriptional repressor Jdp2 and inhibition of actin polymerization, respectively. These findings clearly suggest a role for Dectin-1-mediated sensorine pathways in the resolution of fungal osteoinflammation.

INTRODUCTION

The number of immunosuppressed patients, which includes individuals undergoing organ transplantation, anti-cancer drug treatment, or immunosuppressive therapy or those with HIV/AIDS, has increased significantly in recent years. As a result of advances of emergency medicine, most immunosuppressive complications no longer pose a threat to patients. However, this has caused an increase in various opportunistic infections. Notably, *Candida albicans* infection is one of the major fungal infections observed in immunosuppressed patients (Kullberg and Arendrup, 2015; Pfaller and Diekema, 2004; Yapar, 2014).

Osteomyelitis, an infection characterized by severe inflammation and bone destruction, is difficult to treat. It is well recognized that *C. albicans* can also enter skeletal tissue through a skin wound or by contamination during orthopedic surgery (Arias et al., 2004; Miller and Mejicano, 2001; Rodríguez et al., 2003). Although invasive fungal infections are increasing in immunodeficient hosts, osteomyelitis caused by fungi is a relatively rare infection. However, *C. albicans* osteomyelitis is associated with significant morbidity, and a recent study suggested that it has been reported with increasing frequency from 1970 to 2011 (Gamaletsou et al., 2012). Thus, understanding the pathogenesis of *C. albicans* osteomyelitis is an important issue in the field of orthopedics and osteoimmunology.

It is well established that nociceptor innervation occurs in skin and bone. The function of nociceptors in the osteo-immune system is unclear, but ion channels expressed in the dorsal root ganglia (DRG) are thought to be responsible for sensing noxious stimuli (Woolf and Costigan, 1999). Nav1.8 is a TTX-resistant voltage-gated sodium channel expressed in DRG that is involved



(legend on next page)

in nociception (Zimmermann et al., 2007). Transient receptor potential (TRP) channels are also key players in nociception; in particular, TRP cation channel subfamily V member 1 (TRPV1) and TRP cation channel subfamily A member 1 (TRPA1) are critical channels that mediate nociceptive signaling (Julius, 2013). Recently, it has been reported that nociceptors modulate gram-negative bacterial infections via neuropeptides (Chiu et al., 2013). Capsaicin injection into animals leads to osteoporosis (Ding et al., 2010). Thus, nociceptors may modulate the osteo-immune system, but the mechanism by which they modulate fungal osteomyelitis remains largely unknown.

Fungal cell walls are composed of β -glucan on the inner surface and mannan on the outer surface (Gow et al., 2011). Innate immune cells recognize fungal mannan mainly through Toll-like receptors (TLRs), leading to the production of cytokines via MyD88 and TRIF (Underhill and Iliev, 2014). Mannan is also recognized by the mannose receptor, Dectin-2, DC-SIGN, and Mincle on innate immune cells (Lionakis and Netea, 2013). During budding growth, β -glucan is exposed to the fungal surface or secreted and is sensed by Dectin-1 (Saijo et al., 2007). Dectin-1 induces signaling via the ITAM-like motif, leading to the CARD-9/Bcl-10/Malt-1 trimer and inducing nuclear factor- κ B (NF- κ B) activation (Underhill and Iliev, 2014).

In this study, we discovered that selective depletion of Nav1.8-positive nociceptors leads to exaggerated *C. albicans*-induced inflammation and bone destruction. *C. albicans*-derived β -glucan activates Nav1.8-positive nociceptors via the Dectin-1-TRPV1/TRPA1 axis, leading to the production of calcitonin gene-related peptide (CGRP). Notably, CGRP inhibited β -glucan-induced cytokine production and bone resorbing osteoclasts via inhibition of NF- κ B p65 by the transcriptional repressor Jdp2 and inhibition of actin polymerization, respectively.

RESULTS

Osteoporotic Phenotype of Pain-Nerve-Ablated Mice

To evaluate the function of nociceptor-mediated bone homeostasis, we analyzed the osteo-immune system of resiniferatoxin (RTX)-treated mice (TRPV1-positive neuron ablation; Figures 1A–1C) and *Nav1.8CreRosa26DTA* mice. Both types of mice had normal myeloid and lymphoid populations in splenocytes, but bone volume per tissue volume in distal femurs was significantly impaired (Figures 1D–1F and 1J–1L). Osteoclast parame-

ters were increased in both types of mice, indicating that the absence of nociceptors negatively affects osteoclast generation in vivo (Figures 1G–1I and 1M–1O). Collectively, these findings suggest that nociceptors have the ability to protect bone.

Nav1.8-Positive Pain Nerve Ablation Increases Fungal Osteoinflammation

To visualize Nav1.8-positive nociceptors, we generated *Nav1.8Cre Rosa 26 tdRFP* mice. Fluorescence microscope analysis revealed that Nav1.8-positive nociceptors are innervated into calcaneus (Figure S1A). Intriguingly, Dectin-1, a *C. albicans* and β -glucan receptor, was expressed in nociceptors such as DRG and trigeminal ganglion (Figure S1B). To evaluate the function of nociceptor-mediated fungal osteoinflammation, we next injected *C. albicans* or *C. albicans*-derived soluble β -glucan (CSBG) (Ishibashi et al., 2002) into RTX-treated mice and *Nav1.8CreRosa26DTA* mice. After *C. albicans* or CSBG injection into the hindpaw, both mice showed dramatically increased footpad swelling, serum tumor necrosis factor alpha (TNF- α) levels, calcaneus surface erosion, and serum bone destruction marker levels compared with control mice (Figures 2A–2C). Histological analysis of the calcaneus from CSBG-injected *Nav1.8CreRosa26DTA* mice revealed a dramatic increase in osteoclast numbers (Figures 2D and 2E). Interleukin-23 (IL-23) and IL-17 cytokine expression and fungal burden were normal in *C. albicans*- or CSBG-injected hindpaws of *Nav1.8CreRosa26DTA* mice (Figures S1C and S1D). When we intravenously injected neutralizing TNF- α antibody into CSBG-treated wild-type mice, hindpaw swelling and calcaneus bone destruction were significantly impaired compared with control immunoglobulin G (IgG)-injected wild-type mice (Figures 3A–3C). Depletion of T cells using anti-CD3 antibody did not affect CSBG-induced hindpaw inflammation or bone destruction (Figures S2A and S2B). In contrast to CSBG injection, *Nav1.8CreRosa26DTA* mice that received a lipopolysaccharide (LPS) injection into the hindpaw showed a mild increase in footpad swelling compared with control mice (Figures 3D–3F). Differences in hindpaw TNF- α and IL-6 expression between wild-type and *Nav1.8CreRosa26DTA* mice were more significant in response to CSBG injection than LPS injection (Figure 3G). Despite normal cytokine production by neutrophils in response to various fungal or bacterial components (Figure 3H), *Nav1.8CreRosa26DTA* mice are highly susceptible to the

Figure 1. Osteoporotic Phenotype of RTX-Treated and *Nav1.8CreRosa26DTA* Mice

- (A) RTX treatment protocol.
 (B) Wiping behavior analysis after cheek injection of capsaicin administered to RTX-treated mice (n = 5).
 (C) TRPV1 and TRPA1 expression levels in DRG from RTX-treated and control mice (n = 3).
 (D) Splenocytes from RTX-treated mice were analyzed by fluorescence-activated cell sorting (FACS).
 (E) Representative μ CT images of distal femurs (left) and the metaphyseal portion of femurs (right) from RTX-treated mice.
 (F and G) Bone morphometric analysis of distal femurs by μ CT (F). Bone histomorphometric analysis of the metaphyseal portion of tibias (G; n = 5–6).
 (H and I) In vitro osteoclastogenesis and pit formation in RTX-treated mice (H). Tartrate-resistant acid phosphatase (TRAP) expression levels and pit areas (%) were quantified (I).
 (J) Splenocytes from *Nav1.8CreRosa26DTA* mice were analyzed using FACS.
 (K) Representative μ CT images of distal femurs (left) and the metaphyseal portion of femurs (right) from *Nav1.8CreRosa26DTA* mice.
 (L and M) Bone morphometric analysis of distal femurs by μ CT (L). Bone histomorphometric analysis of the metaphyseal portion of tibias (M; n = 5–6).
 (N and O) In vitro osteoclastogenesis and pit formation in *Nav1.8CreRosa26DTA* mice (N). TRAP expression levels and pit areas (%) were quantified (O).
 Error bars represent SE. *p < 0.05, **p < 0.01. BV/TV, bone volume per tissue volume; Tb.Th, trabecular bone thickness; Tb.N, trabecular bone number; Tb.Sp, trabecular bone spacing; Oc.S/BS, osteoclast surface per bone surface; Oc.N/BS, osteoclast number per bone surface; Ob.S/BS, osteoblast surface per bone surface; Ob.N/BS, osteoblast number per bone surface; BFR/BS, bone formation rate per bone surface; MAR, mineral apposition rate.

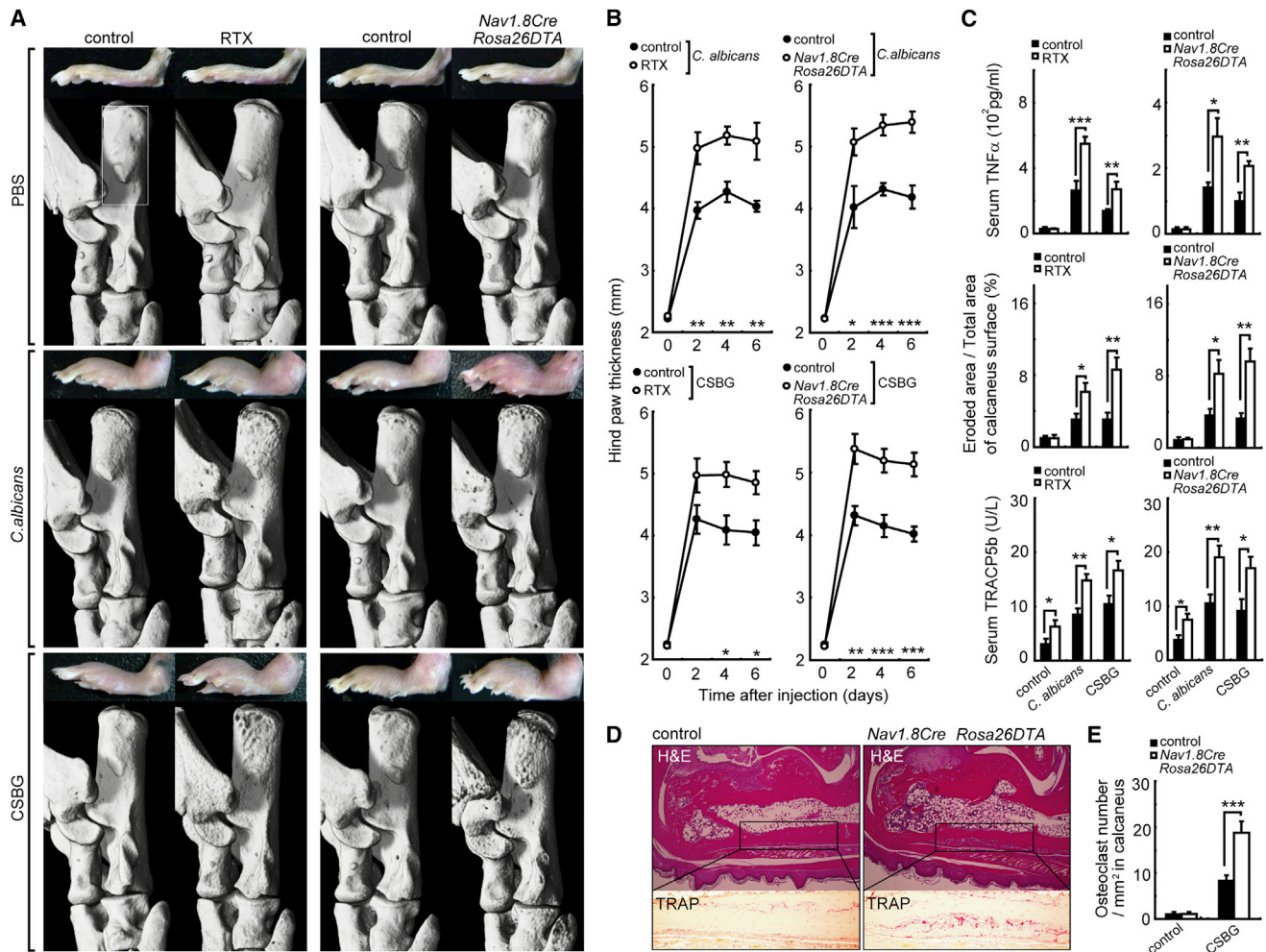


Figure 2. Nociceptors Protect from Increased Osteoinflammation in Response to *C. albicans* or β -Glucan

(A–E) *C. albicans* (3×10^7 colony-forming units [CFUs]) or CSBG (150 μ g) was injected into the hindpaws of RTX-treated denervated or *Nav1.8CreRosa26DTA* mice. (A) Hindpaws and ankle μ CT images at day 6 after injection. (B) Sequential hindpaw thickness. (C) Serum TNF- α levels, eroded area/total area of calcaneus surface (%), and serum TRACP5b levels in (A) at day 6 after injection. (D) Representative calcaneus histology from *Nav1.8CreRosa26DTA* mice at day 6 after CSBG injection (TRAP staining indicates osteoclasts). (E) Osteoclast number per square millimeter in calcaneus in (D) ($n = 8$ /group). Error bars represent SE; * $p < 0.05$; ** $p < 0.01$; *** $p < 0.001$; ns, not significant.

intraperitoneal injection of the Dectin-1 ligand Curdlan, but not to LPS (Figures 3I–3L). Thus, Dectin-1-mediated osteoinflammation, but not TLR4-mediated osteoinflammation, is potently suppressed by nociceptors.

β -Glucan Induces Robust CGRP Secretion from Sensory Nerves through the Dectin1-PLC-TRPV1/TRPA1 Axis

Pain nerves express neuropeptides such as neurokinin A, substance P, galanin, somatostatin, and CGRP. CGRP is the only one of these peptides that is secreted into the serum or synovial tissue after *C. albicans* injection into the hindpaw (Figures 4A and 4B). Because CGRP inhibits TLR4 signaling (Nong et al., 1989) and is present at high levels in DRG neurons but barely detectable in other tissues or cells (Figure 4C), we hypothesized that Dectin-1-stimulated DRG neurons inhibit osteo-inflammation via CGRP production. In vitro analysis revealed that CGRP is

released from DRG neurons in response to CSBG or heat-killed (hk) *C. albicans*, and this secretion was dependent on extracellular Ca^{2+} , phospholipase C (PLC), and Dectin-1 (Figure 4D). TRPV1 or TRPA1 single-deficient DRG neurons showed partial, and TRPV1/TRPA1 double-deficient DRG neurons showed severe, impairment of CGRP production in response to CSBG or hk *C. albicans* stimulation (Figure 4D). Constitutive serum CGRP levels were lower in *Nav1.8CreRosa26DTA* mice than in control mice (Figure 4E). After hindpaw injection of hk *C. albicans* or CSBG, serum CGRP induction was significantly impaired in RTX-treated mice and *Nav1.8CreRosa26DTA* mice compared with control mice (Figure 4E). Dectin-1-deficient or PLC-inhibitor-treated mice also showed severely impaired serum CGRP induction in response to hindpaw CSBG injection (Figure 4F). By contrast, Bcl-10- or Malt-1-deficient mice showed normal serum CGRP production in response to CSBG

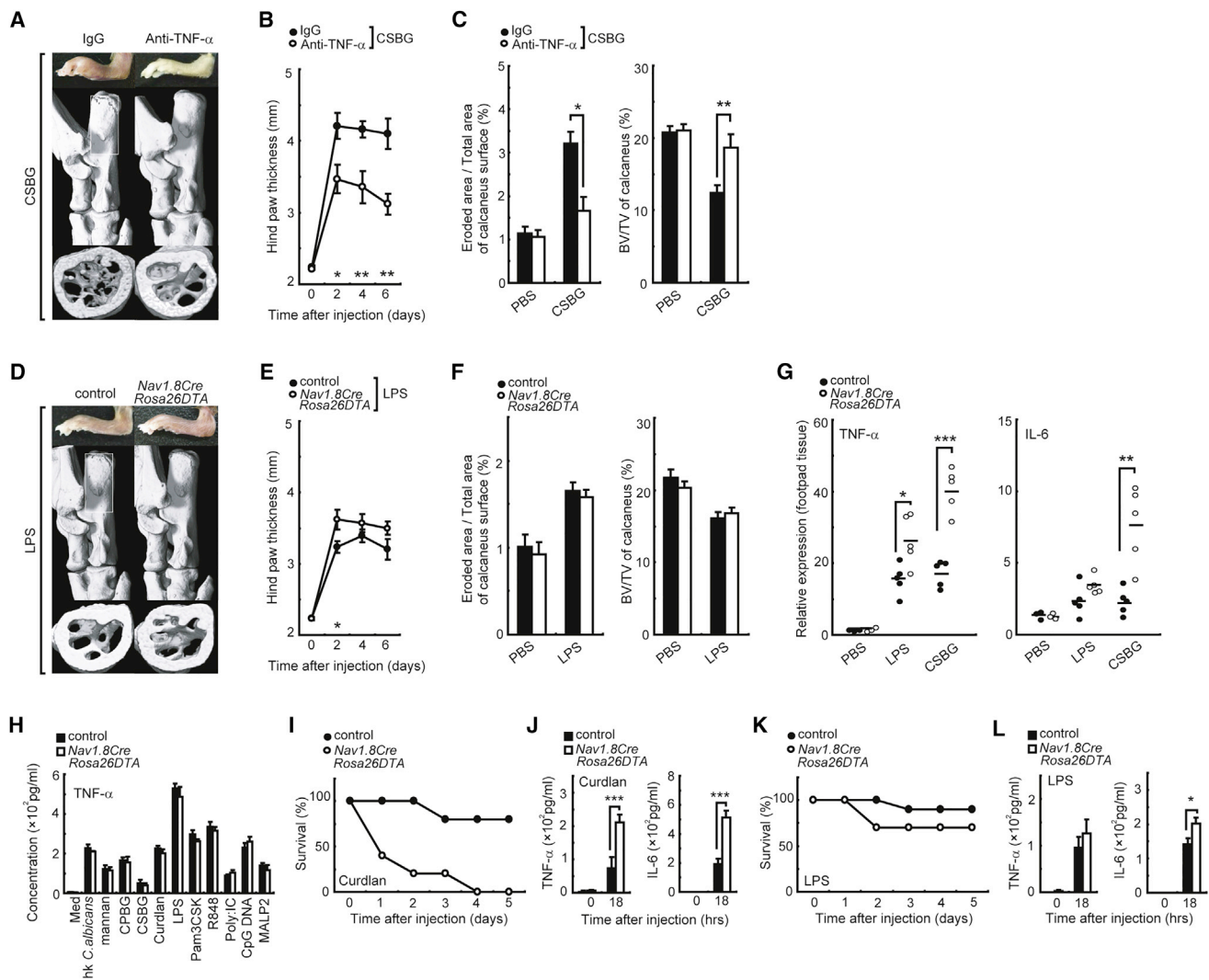


Figure 3. β -Glucan-Mediated Osteoinflammation, but Not TLR4-Mediated Osteoinflammation, Is Potently Suppressed by Nav1.8-Positive Nociceptors

(A–C) To neutralize TNF- α , an anti-TNF- α antibody or isotype control antibody were intraperitoneally injected. After 12 hr, CSBG (150 μ g) was injected into the hindpaws of mice. Representative images of the hindpaws (top), ankle μ CT images (middle), and the axial view of calcaneus μ CT images (bottom) at day 6 after CSBG injection are presented in (A). Sequential hindpaw thickness is shown in (B). Eroded area/total area of the calcaneus surface (%) and BV/TV of the calcaneus in (A) are indicated in (C) (n = 8).

(D–F) LPS (150 μ g) was injected into hindpaws of Nav1.8CreRosa26DTA mice. Representative pictures of hindpaws (top), ankle μ CT images (middle), and the axial view of calcaneus μ CT images (bottom) at day 6 after LPS injection are presented (D). Sequential hindpaw thickness is shown in (E). Eroded area/total area of the calcaneus surface (%) and BV/TV of the calcaneus in (F) are indicated in (G) (n = 8).

(G) LPS or CSBG was injected into the hindpaws of Nav1.8CreRosa26DTA mice. After 6 days, TNF- α and IL-6 expression levels in the hindpaw tissues were analyzed using qPCR (n = 5).

(H) Neutrophils from Nav1.8CreRosa26DTA mice were collected and stimulated by various fungal and bacterial components. After 24 hr, TNF- α levels in the supernatant were measured (n = 5).

(I and J) Curdlan was intraperitoneally injected into Nav1.8CreRosa26DTA mice, and survival was monitored (I). Serum cytokine levels were determined 18 hr after injection (J; n = 5).

(K and L) LPS was intraperitoneally injected into Nav1.8CreRosa26DTA mice and survival was monitored (K). Serum cytokine levels were determined 18 hr after injection (L; n = 10).

Error bars represent SE; *p < 0.05; **p < 0.01; ***p < 0.001.

(Figure 4F). TRPV1 or TRPA1 single-deficient mice showed partial, and TRPV1/TRPA1 double-deficient mice showed significant, impairment of serum CGRP levels in response to hindpaw injection of CSBG or *hk C. albicans* (Figure 4F). CGRP co-administra-

tion into the hindpaw reversed the hyperinflammatory and bone-destructive phenotype in Nav1.8CreRosa26DTA mice in response to CSBG (Figures S2A and S2B). Reflecting the weak inhibitory effect of LPS-induced inflammation in pain nerves, an increase in

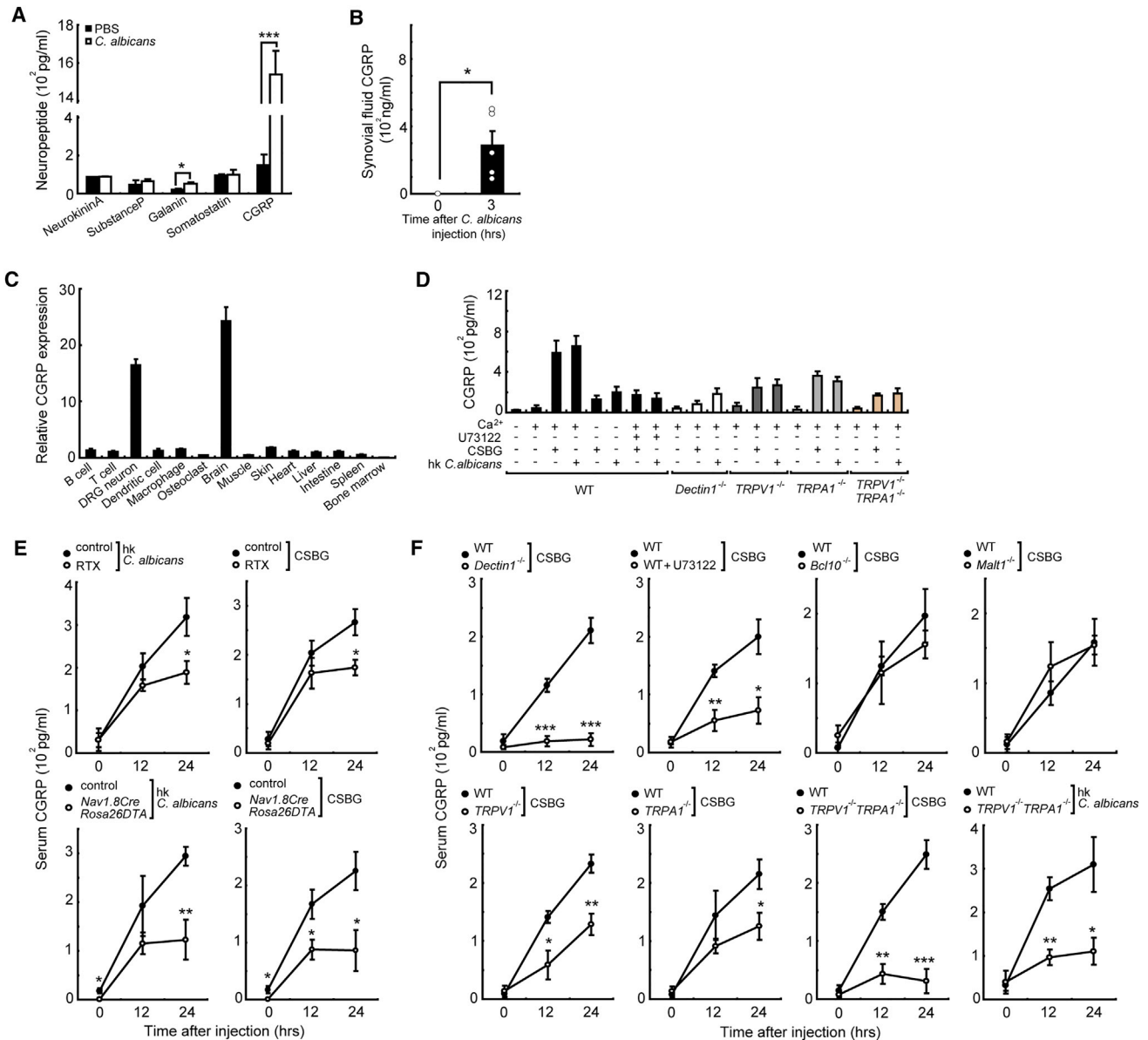


Figure 4. β -Glucan-Induced CGRP Production in Serum Is Dependent on the Dectin-1-PLC-TRPV1/TRPA1 Axis

(A and B) ELISA analysis of serum (A) or synovial fluid (B) neuropeptide levels in WT mice injected with *C. albicans* (3×10^8 CFUs/25 μ L) (n = 4–5).

(C) Relative CGRP expression levels (n = 3).

(D) CGRP levels in the culture supernatant from DRG neurons cultured for 24 hr with or without Ca²⁺-containing medium and U73122 (10 μ M) and stimulated by CSBG or heat-killed (hk) *C. albicans* (n = 3).

(E) Serum CGRP levels in denervated mice (RTX-treated mice or Nav1.8Cre Rosa 26DTA mice) injected with hk *C. albicans* (3×10^7 CFUs/25 μ L) or CSBG (150 μ g/25 μ L) (n = 4/group).

(F) Serum CGRP levels in various knockout mice injected with hk *C. albicans* (3×10^7 CFUs/25 μ L) or CSBG (150 μ g/25 μ L) (n = 4/group).

Error bars represent SE; *p < 0.05; **p < 0.01; ***p < 0.001.

serum CGRP in response to hindpaw CSBG or Curdlan injection was stronger and more sustained than that produced by LPS injection (Figures S2C and S2D). Finally, we tested whether loss of TRPV1 and/or TRPA1 deficiency altered the osteo-immune response to β -glucan. TRPV1 and/or TRPA1 deficiency showed normal bone metabolism and hematopoiesis (Figures S3A–S3C). In vitro receptor activator of NF- κ B ligand (RANKL) and

TNF- α -induced osteoclastogenesis in these mice was also unaltered compared with wild-type controls (Figures S3D and S3E). Despite normal cytokine production in myeloid cells in response to various fungal or bacterial components (Figures S3F and S3G), TRPV1/TRPA1 double-deficient mice showed significantly enhanced hindpaw swelling, serum IL-6 concentration, and calcaneus bone destruction in response to CSBG injection into

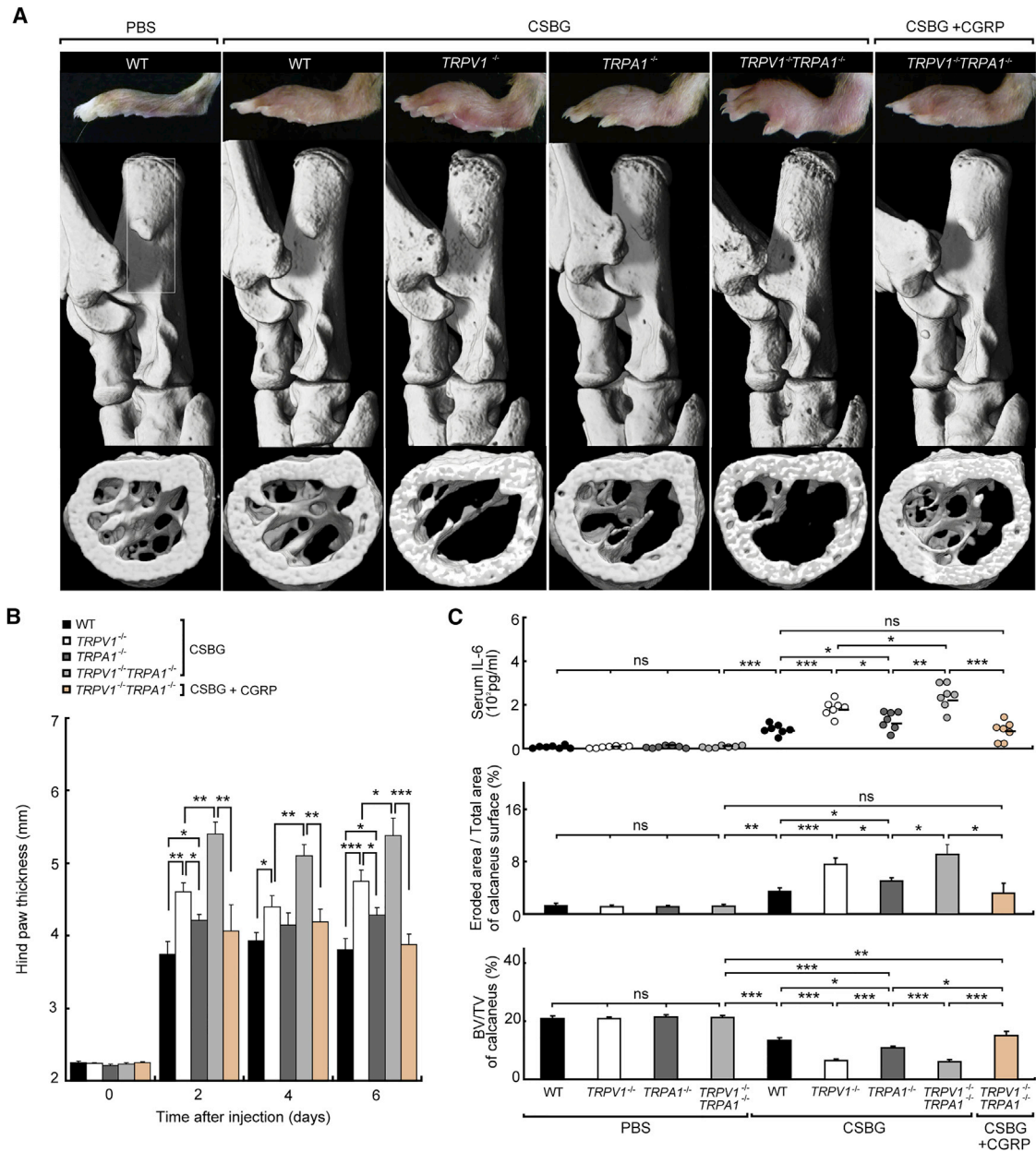


Figure 5. TRPV1/TRPA1 Protects from Osteoinflammation Induced by β -Glucan

CSBG (150 μ g) was injected into the hindpaws of wild-type (WT), *TRPV1*^{-/-}, *TRPA1*^{-/-}, and *TRPV1*^{-/-}*TRPA1*^{-/-} mice. *TRPV1*^{-/-}*TRPA1*^{-/-} mice were concurrently injected with CGRP.

(A) Representative images of the hindpaws (upper), calcaneus surface μ CT images (middle), and the trabecular area of calcaneus μ CT images (lower) at day 6 after injection.

(B) Sequential hindpaw thickness.

(C) Serum IL-6 levels, the eroded area/total area of the calcaneus surface (%) in (A), and the bone volume/tissue volume of the calcaneus (%) in (A) (n = 7). Error bars represent SE; *p < 0.05; **p < 0.01; ***p < 0.001.

the hindpaw (Figures 5A–5C). *TRPV1* or *TRPA1* single-knockout mice also showed enhanced osteoinflammation in response to CSBG, and the relative contribution of each TRP channel to the phenotypes observed in double-knockout mice was more significant with *TRPV1* (Figures 5A–5C). Strikingly, CGRP injection with

CSBG reversed the hyper-inflammatory and bone destructive phenotype of *TRPV1*/*TRPA1* double-deficient mice (Figures 5A–5C). These findings clearly indicated that Dectin-1-PLC-*TRPV1*/*TRPA1*-axis-induced CGRP secretion from the sensory nerves controls the resolution of fungal osteoinflammation.

Pain-Nerve-Derived CGRP Inhibits Osteoclast Multinucleation, but Not Differentiation

To test the potential role of neuropeptides in osteoclast formation, we screened pain nerves expressing neuropeptides in RANKL-induced osteoclastogenesis. Compared with the PBS control, only CGRP inhibited osteoclast multinucleation and bone-resorptive activity (Figures 6A–6F). In contrast to the severe impairment of osteoclastogenesis, osteoclast marker expression, such as that of Jdp2 (Maruyama et al., 2012a), remained unchanged (Figure 6C), and RANKL-induced Jdp2 induction was not affected by Dectin-1 signaling (Figure 6G). We also quantified expression of the various osteoclast-associated genes and apoptosis levels in CGRP-treated osteoclasts, but all remained unchanged (Figures 6H and 6I). Neurokinin A caused a slight increase in osteoclast differentiation (Figures 6A–6C) that required further analysis. Of all neuropeptides tested, CGRP treatment was the most potent inhibitor of osteoclasts. Importantly, expression of CGRP receptors, such as RAMP1 and CALCRL, was detected in osteoclasts (Figures S4A, S4B, and S4D). Combination treatment of macrophages with CGRP and RANKL caused time-dependent cyclic AMP (cAMP) accumulation, which was not seen in RANKL single stimulation (Figure 6J), and the RANKL-induced Jdp2 increase was not affected by CGRP or cAMP co-stimulation (Figure 6K). Because cAMP has been reported to modulate F-actin polymerization, we compared CGRP and cAMP effects on osteoclast actin belt formation. CGRP started to destroy the osteoclast actin belt at 3 hr, and it was eliminated at 12 hr (Figure 6L). The importance of cAMP for the CGRP effect on actin belt de-polymerization suggests that cAMP mimics the effect of CGRP (Figure 6L). The DRG culture supernatant inhibited osteoclast multinucleation, and treatment with olcegepant, a CGRP receptor antagonist, reversed this effect (Figure 6M). Thus, we conclude that pain-nerve-derived CGRP inhibits actin polymerization via cAMP induction, leading to the impairment of osteoclast multinucleation (Figure 7I).

Pain-Nerve-Derived CGRP Inhibits β -Glucan-Induced Inflammation via the Transcriptional Repressor Jdp2

We screened neuropeptides to analyze their effects on TNF- α production from hk *C. albicans*-stimulated macrophages and revealed that only CGRP had the potential to inhibit TNF- α production (Figure 7A). Notably, CGRP receptors, such as RAMP1 and CALCRL, were expressed on myeloid cells, and *C. albicans* infection upregulated the expression of CALCRL (Figures S4A–S4C). Because CGRP inhibited CSBG and *C. albicans*-derived particulate β -glucan (CPBG)-induced (Ishibashi et al., 2002) TNF- α production more strongly than mannan (Figure 7B), we hypothesized that CGRP mainly suppresses Dectin-1 signaling rather than TLR signaling. Because the transcriptional repressor Jdp2 is not induced by LPS but represses the transcriptional activities of various transcription factors (Maruyama et al., 2012a), we compared Jdp2 induction levels in response to *C. albicans* components. Mannan, CPBG, or CSBG single stimulation could not induce Jdp2 expression, but addition of CGRP with CPBG or CSBG significantly induced Jdp2 (Figure 7C). The addition of cAMP to mannan, CPBG, or CSBG also significantly stimulated Jdp2 induction (Figure 7C). CPBG stimulation alone did not

induce cAMP induction, but CPBG plus CGRP stimulation induced cAMP induction, indicating that Dectin-1 plus CGRP signaling is required for cAMP-mediated Jdp2 induction (Figure 7D). Myeloid cells from Jdp2-deficient mice showed normal TNF- α and IL-6 production in response to Dectin-1 stimulation (Figures 7E and S5A). However, CGRP- or cAMP-mediated suppression of TNF- α and IL-6 production in response to Dectin-1 stimulation was completely abolished in Jdp2-deficient myeloid cells (Figure 7E). Serum CGRP concentrations were significantly elevated, and serum CGRP increases in response to CSBG hind-paw injection were significantly higher, in Jdp2-deficient mice than in wild-type mice (Figure S5B). Hindpaw swelling and IL-6 concentrations in serum were also elevated, and RTX denervation or CGRP injection did not influence the CSBG-induced hyper-inflammatory phenotype of Jdp2-deficient mice (Figures S5C–S5E). Chimeric wild-type mice lacking Jdp2 in their hematopoietic system showed enhanced footpad swelling and serum cytokine levels in response to CSBG (Figures S5F–S5H). Conversely, chimeric knockout mice possessing wild-type bone marrow showed a normal inflammatory phenotype (Figures S5F–S5H). Thus, enhanced Dectin-1-mediated inflammation in Jdp2-deficient mice may be a result of unresponsiveness to CGRP in the hematopoietic system. To gain insight into the mechanism underlying Jdp2-mediated cytokine suppression, we first examined NF- κ B p65 activation in response to CPBG alone or CPBG plus CGRP, revealing that p65 DNA binding to its promoter was not impaired in CPBG-plus-CGRP-treated Jdp2-deficient macrophages (Figure 7F). Importantly, an association between Jdp2 and p65 was identified by immunoprecipitation (Figure 7G). CPBG- or CSBG-induced p65 binding to the TNF- α promoter was suppressed by CGRP or cAMP treatment and by Jdp2 overexpression (Figure 7H). Conversely, RANKL-induced p65 binding to the promoter of NFATc1, a master regulator of osteoclastogenesis, was not altered by Jdp2 overexpression (Figure 7H). These findings indicated that CGRP-induced Jdp2 in myeloid cells selectively blocks Dectin-1-mediated pro-inflammatory cytokine production by direct p65 inhibition (Figure 7I).

DISCUSSION

In both skin and bone, Nav1.8-positive nociceptors seem to be the primary source of CGRP. CGRP suppressed β -glucan-induced cytokine production from myeloid cells and RANKL-induced osteoclast multinucleation via the induction of the transcriptional repressor Jdp2 and cAMP, respectively (Figure 7I). Recent reports suggest that denervated mice showed impaired IL-23/IL-17-mediated skin inflammation in response to *C. albicans* (Kashem et al., 2015). However, we did not detect any differences in IL-23/IL-17 levels or fungal burden in *Nav1.8CreRosa26DTA* mice injected with *C. albicans*, and they showed severe paw inflammation and bone destruction compared with controls. Discrepancies between our findings and a previous report may be explained by the difference in the denervation method used for nociceptors or fungal strains. To generate denervated mice, the previous report mechanically disrupted the cutaneous nerves on one lateral half of the mouse dorsum (Kashem et al., 2015). By contrast, we used targeted

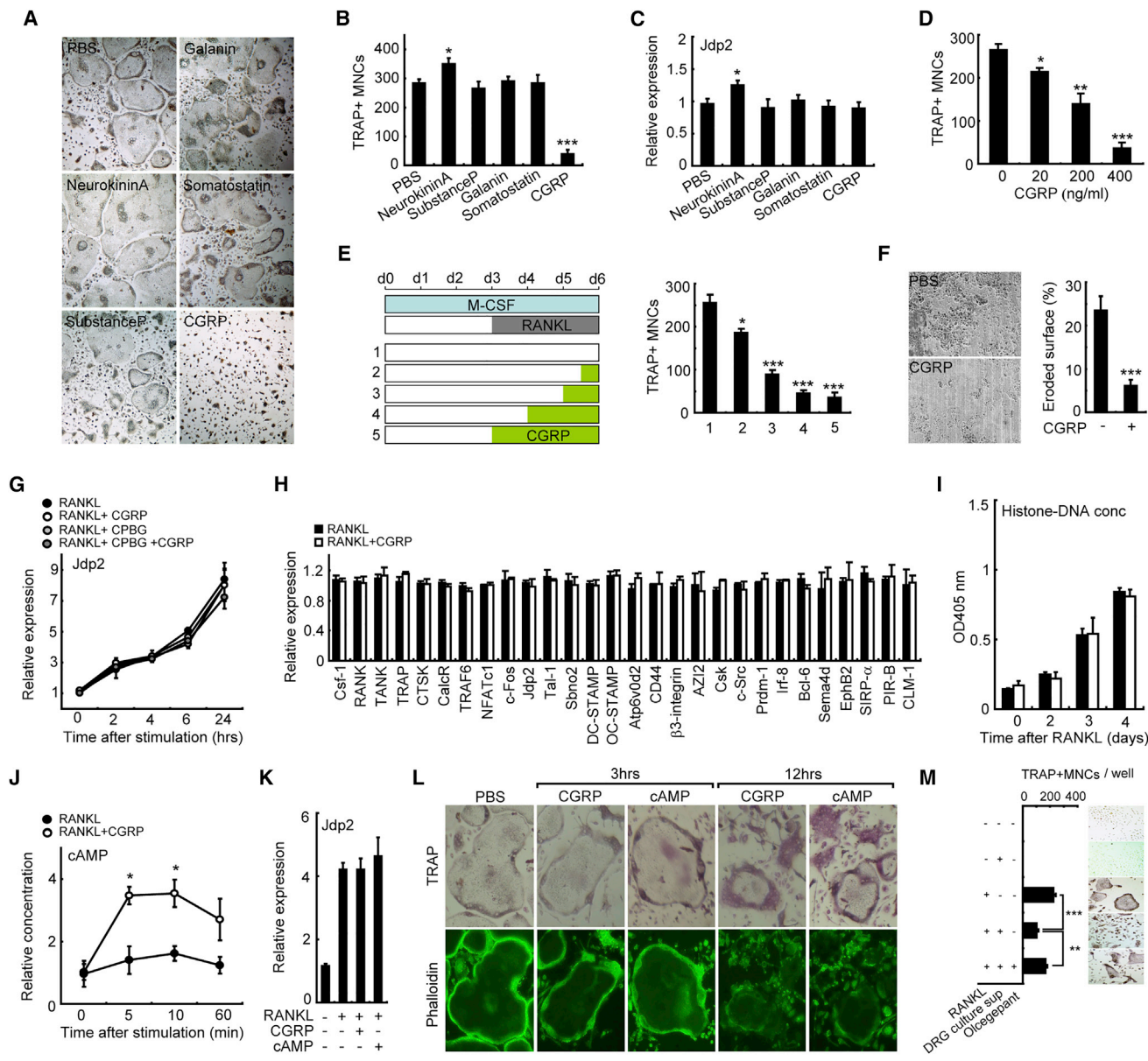


Figure 6. CGRP Inhibits Osteoclast Multinucleation, but Not Differentiation

(A) TRAP staining of osteoclasts in M-CSF-derived macrophages (MDMs) cultured with the indicated neuropeptides (400 ng/mL) plus RANKL for 3 days. (B) Numbers of TRAP⁺ multi-nucleated cells (MNCs) in (A) (n = 5). (C) qPCR quantification of Jdp2 expression in cultured MDMs (n = 3). (D) Dose-dependent inhibition of osteoclastogenesis by CGRP (n = 5). (E) TRAP⁺ MNC count in bone marrow cells cultured under five different conditions for 6 days (n = 5). (F) Scanning electron microscopic quantification of the dentine slice surface eroded by osteoclasts cultured with or without CGRP (n = 8). (G) MDMs were stimulated by RANKL (75 ng/mL), CPBG (100 μg/mL), and CGRP (400 ng/mL). Jdp2 expression levels were quantified using qPCR (n = 3). (H) MDMs were stimulated with RANKL and CGRP. After 3 days, osteoclast-associated gene expression levels were quantified by qPCR (n = 3). (I) MDMs were stimulated with RANKL and CGRP. Culture supernatant concentrations of histone DNA were measured (n = 3). (J) MDMs were stimulated with RANKL plus CGRP. cAMP levels in MDMs were quantified (n = 3). (K) MDMs were stimulated with RANKL, CGRP, and cAMP (10 μM). After 5 hr, Jdp2 expression levels were quantified by qPCR (n = 3). (L) MDMs were stimulated with RANKL for 3 days to generate osteoclasts. Cells were then treated with CGRP and cAMP for 3 or 12 hr. TRAP and phalloidin staining was performed to visualize osteoclasts and actin belt formation, respectively (n = 3). (M) DRG from WT mice were cultured in αMEM supplemented with 10% FCS. After 48 hr, culture supernatants were harvested (DRG culture sup). MDMs were cultured with RANKL, DRG culture supernatant, and olcegepant (CGRP receptor agonist). After 3 days, osteoclast numbers were counted (n = 6). Error bars represent SE; *p < 0.05; **p < 0.01; ***p < 0.001.

diphtheria-toxin-based nociceptor ablation to explore the role of Nav1.8 positive nociceptors. Thus, Nav1.8-negative nociceptors may function to stimulate IL-17 and IL-23 expression in response to β -glucan. Further nociceptor-type-specific studies are needed to clarify the importance of pain neurons in fungal infections.

Recently, it has been reported that *Staphylococcus aureus* skin infection directly activates nociceptors and that Nav1.8-positive nociceptors suppress hindpaw inflammation (Chiu et al., 2013). Like *S. aureus*, *C. albicans* may directly stimulate nociceptors and evoke anti-inflammatory function. In this study, we also discovered that Dectin-1-mediated osteoinflammation, but not TLR4-mediated osteoinflammation, is potently suppressed by nociceptors. Strikingly, β -glucan-induced CGRP production from nociceptors was more potent than that induced by LPS. Thus, nociceptors may function mainly in fungal inflammation rather than in gram-negative bacterial inflammation.

Cross-talk between CGRP and Dectin-1 signaling in myeloid cells was responsible for the cAMP-mediated Jdp2 induction, causing suppression of inflammation. A significant discovery in this study is that Jdp2 physically binds to p65 and reduces p65 recruitment to the cytokine promoter. Jdp2 is a member of the AP-1 family of genes (c-Fos, Fra1, and Fra2), which are generally thought to be involved in suppression of TLR-mediated inflammation (Kim et al., 2005). However, Jdp2 is likely to be suppressive toward p65 only after β -glucan plus CGRP stimulation, because mannan plus CGRP stimulation did not induce Jdp2. These findings are consistent with results showing that the Jdp2 deficiency hyper-inflammatory phenotype induced by CSBG was only observed in vivo.

In this study, we investigated how TRPV1/TRPA1 regulates the fungal osteoinflammation process. *Nav1.8CreRosa26DTA* mice showed impaired serum CGRP levels, causing reduced bone volume that results from increased osteoclastogenesis. By contrast, bone volume and CGRP levels in serum were normal in TRPV1- and/or TRPA1-deficient mice, suggesting that both ion channels are not involved in constitutive CGRP production. However, after CSBG injection into the hindpaw, serum CGRP induction was abolished in TRPV1/TRPA1 double-deficient mice, indicating that both ion channels are required for “emergency” CGRP induction. In vitro cytokine production or osteoclastogenesis in myeloid cells from TRPV1- and/or TRPA1-deficient mice were

normal, and the levels of emergency CGRP induction in these mice may negatively correlate with in vivo inflammation. Further studies are required to reveal the mechanisms of TRP-channel-mediated CGRP production in nociceptors.

In this study, we discovered that Nav1.8-positive nociceptors may function as protectors of fungal osteoinflammation via “emergency” CGRP production (Figure 7I). Thus, in the context of fungal infection, Nav1.8-positive nociceptors are “regulatory neurons,” and strategies to enhance CGRP secretion or Jdp2 activation might be beneficial to preventing the complications of β -glucan-associated inflammation or bone destruction. Despite these findings, the clinical implications of these denerivated mouse phenotypes are still enigmatic. Congenital insensitivity to pain with anhidrosis is an extremely rare hereditary disease characterized by impairment of nociceptor development. Manifestations of congenital insensitivity to pain with anhidrosis are recurrent episodes of skin injury, osteomyelitis, bony fractures, and oral osteolysis (Butler et al., 2006; Swanson, 1963; Zhang and Haga, 2014). Precise microbiological observation of this rare disease may clarify the bona fide role of human nociceptors in fungal infection.

EXPERIMENTAL PROCEDURES

Mice

For in vivo experiments, 8- to 13-week-old female mice were used. *Bcl-10^{-/-}* mice and *Malt-1^{-/-}* mice were a gift from S. Gerondakis, S. Morris, and V.M. Dixit, respectively (Ruefli-Brasse et al., 2003; Xue et al., 2003) and were compared with WT littermate controls. *Dectin1^{-/-}* mice (Saijo et al., 2007), *Jdp2^{-/-}* mice (Maruyama et al., 2012a), and *TLR4^{-/-}* mice (Hoshino et al., 1999) were generated as described and were compared with WT littermate controls. *TRPV1^{-/-}* mice (Caterina et al., 2000) and *TRPA1^{-/-}* mice (original strain was backcrossed for more than eight generations with C57BL/6) (Bautista et al., 2006) were generated as described and control C57BL/6 mice were purchased from SLC. *Rosa26-tdRFP* reporter mice were generated as described previously (Luche et al., 2007). Sperm from *Nav1.8-Cre* mice (B6;129-Scn10atm(cre)Jnw/H, stock ID EM:04582) was purchased from the European Mouse Mutant Archive, and in vitro fertilization was performed. *Rosa26-DTA* mice (B6;129-Gt26Sortm1(DTA)Mrc/J, stock number 010527) were purchased from Jackson Laboratory. *Nav1.8-Cre* mice were bred with *Rosa26-tdRFP* reporter mice to generate *Nav1.8Cre Rosa26-tdRFP* mice. *Nav1.8-Cre^{+/-}* mice were bred with C57BL/6 *Rosa26-DTA^{+/+}* mice to generate pain-nerve-deficient mice (*Nav1.8Cre^{+/-} Rosa26-DTA^{+/-}*) and littermate controls (*Nav1.8Cre^{-/-} Rosa26-DTA^{+/-}*) (Abrahamsen et al., 2008). Animal experiments complied with the institutional animal care and use guidelines of Osaka

Figure 7. CGRP Inhibits β -Glucan-Induced Cytokine Production via Transcriptional Repressor Jdp2

- (A) TNF- α levels in the supernatant of MDMs stimulated for 24 hr by hk *C. albicans* with the indicated neuropeptides (100 or 400 ng/mL) (n = 3).
 (B) TNF- α levels in the supernatant of neutrophils (Neu), conventional dendritic cells (DC), and MDMs (Mac) from WT or *Dectin1^{-/-}* mice stimulated by mannan (100 μ g/mL), CPBG (100 μ g/mL), or CSBG (100 μ g/mL) with or without CGRP (400 ng/mL) for 24 hr (n = 3).
 (C) qPCR quantification of Jdp2 expression in MDMs stimulated with mannan, CPBG, CSBG, CGRP, and cAMP (10 μ M) for 3 hr (n = 3).
 (D) Jdp2 expression levels and intracellular cAMP levels in MDMs stimulated with CPBG plus CGRP (n = 3).
 (E) TNF- α and IL-6 levels in the supernatant of MDMs from *Jdp2^{-/-}* mice stimulated with the indicated ligands for 24 hr (n = 3).
 (F) NF- κ B p65 DNA binding activity of MDMs stimulated with the indicated ligands for 3 hr (n = 3).
 (G) Immunoprecipitation in 293T cells transfected with the indicated pCMV vectors (top). MDMs were stimulated with CPBG plus CGRP for 3 hr and lysed. After anti-p65 IgG immunoprecipitation, immunoprecipitates were analyzed (bottom).
 (H) Chromatin immunoprecipitation analysis with p65 antibody of the lysates from MDMs. MDMs were infected using a retrovirus encoding Jdp2 (Izr-Jdp2) or an empty control (Izr-empty) and were stimulated with CPBG/CSBG or RANKL for 3 and 24 hr, respectively. CGRP and cAMP were also added as indicated. DNA fragments of the TNF- α promoter region and NFATc1 promoter region were detected by PCR.
 (I) Model for the sensocrine regulation of fungal osteoinflammation. β -Glucan induces robust CGRP secretion from sensory nerves through the Dectin1-PLC-TRPV1/TRPA1 axis, and CGRP inhibits osteoclast multinucleation. Notably, pain-nerve-derived CGRP inhibits β -glucan-induced NF- κ B activation of myeloid cells by the transcriptional repressor Jdp2.

Error bars represent SE; *p < 0.05; **p < 0.01; ***p < 0.001.

University (animal 14013) and the National Institutes of Natural Sciences (16A074).

Generation of Bone Marrow Chimeric Mice

Bone marrow transfer was performed as previously described (Maruyama et al., 2013). Briefly, donor bone marrow cells from *Jdp2*^{-/-} and age-matched control wild-type mice were collected, and 1×10^7 cells were intravenously injected into lethally irradiated 4-week-old recipient mice. Mice were analyzed 7 weeks after bone marrow transplantation.

Denervation by RTX

RTX (R8756, Sigma-Aldrich) was injected subcutaneously into the flank of 4-week-old female C57BL/6 mice at three escalating doses (80 ng/g body weight, 100 ng/g body weight, and 150 ng/g body weight) on consecutive days. Control mice were injected with DMSO containing PBS. Pain-nerve-depleted 8-week-old female mice demonstrated cheek wiping <20 times per 5 min after injection of 50 μ g capsaicin (M2028, Sigma-Aldrich) into the cheek.

Fungal Strain and β -Glucan

C. albicans THK519, designated *C. albicans*, was obtained from a patient admitted to Tohoku University Hospital. CSBG and CPBG were prepared from *C. albicans* NRBC1385, which was purchased from the NITE Biological Resource Center, as previously described (Ishibashi et al., 2002). Additional information on fungal and bacterial strains and on the cells and reagents used is provided in Supplemental Experimental Procedures.

In Vivo Injection of Pathogens and Their Components

Pathogen or ligand injection into the hindpaws of mice was performed as previously described (Chiu et al., 2013; Shimada and LaMotte, 2008). Details on the pathogens and additional information on cell depletion and neutralizing antibodies can be found in Supplemental Experimental Procedures.

DRG Neuron Isolation

The DRGs were separated from L1 to L6 in mice. The DRG neurons were used for experiments between 2 and 6 hr after isolation. Details of the DRG neuron isolation technique are presented in Supplemental Experimental Procedures.

Histological and Radiological Analysis of Bone Tissue

To measure bone formation, double calcein labeling was performed. Tibias were fixed with 70% ethanol before being subjected to histological bone morphometric analysis. Three-dimensional micro-computed tomography (μ CT) analysis of femurs and ankle joints was conducted using a Scan-Xmate RB080SS110 system (Comscan Techno). Bone structural indices were measured using TRI/3D-Bon software (Ratoc System Engineering). Additional information is provided in Supplemental Experimental Procedures.

PCR, Protein Analysis, Immunoprecipitation, and Viral Gene Transfer

RNA was extracted using TRIzol (Invitrogen Life Science Technologies). Reverse transcription was performed using ReverTra Ace (Toyobo). The quantity of mRNA was normalized to 18S rRNA using TaqMan ribosomal control reagent kit (Applied Biosystems). Western blotting was performed as previously described (Maruyama et al., 2012b). For immunoprecipitation, pre-cleared cell lysates were incubated with protein A-Sepharose-containing antibodies for 1 hr. The immunoprecipitates were washed, eluted, and analyzed by western blotting. Chromatin immunoprecipitation was performed as previously described (Maruyama et al., 2013). For viral gene transfer, retroviral packaging was performed using PlatE. Viral gene transduction to MDMs was performed as previously described (Maruyama et al., 2012a). After transduction, MDMs were harvested and replated onto CSBG- or CPBG-containing tissue culture plates. In some experiments, cells were further stimulated with RANKL. Additional information is provided in Supplemental Experimental Procedures.

ELISA

Kits used in this study included TNF- α and IL-6 ELISA kits (R&D Systems), CGRP ELISA kit (CSB-Equation 027706MO, Wuhan Humei Biotech), Galanin ELISA kit (CSB-EL009191MO, Wuhan Humei Biotech), Substance P EIA kit

(583751, Cayman), Neurokinin A EIA kit (EIAM-NEA-1, RayBiotech), Somatostatin EIA kit (EIAM-SOM-1, RayBiotech), and TRACP5b ELISA kit (Immunodiagnostic Systems). Nuclear extracts were prepared as previously described (Maruyama et al., 2015), and DNA-binding activity of NF- κ B p65 was analyzed using an ELISA-based TransAM Transcription Factor Assay Kit (Active Motive).

Statistical Analysis

The difference in mean values between two groups was compared using the Student's t test, and $p < 0.05$ was considered to be significant.

SUPPLEMENTAL INFORMATION

Supplemental Information includes Supplemental Experimental Procedures and five figures and can be found with this article online at <http://dx.doi.org/10.1016/j.celrep.2017.06.002>.

AUTHOR CONTRIBUTIONS

K.M. initiated, designed, and conducted the entire project. T.K., Y.K., B.R.S., H.K., M.M.M., and N.T. designed and conducted the immunological experiments. K.I. and N.O. provided CSBG and contributed to the experimental design. Y.I. provided Dectin-1-deficient mice and conducted animal experiments. Y.T. and M.T. provided TRPV1- and TRPA1-deficient mice and designed the experiments. The manuscript was written by K.M. and Y.T. S.A. supervised the research.

ACKNOWLEDGMENTS

We thank Dr. H.J. Fehling for providing Rosa26-tdRFP reporter mice; Dr. K.J. Ishii and Dr. K. Kobiyama for helping the animal transfer of Dectin-1 knockout mice; K. Shinno for technical assistance; Dr. S. Saijo, Dr. O. Takeuchi, Dr. T. Saitoh, Dr. K. Matsuo, and K. Asakawa for valuable discussions; and E. Kamada for secretarial assistance. This research was supported by grants from the Osaka University MEET project (K.M.), the Takeda Science Foundation ("Visionary Research" to K.M.), the Naito Foundation (to K.M.), a KAKENHI Grant-in-Aid for Challenging Exploratory Research (JP26670663 and JP16K15665 to K.M.), a KAKENHI Grant-in-Aid for Young Scientists A (JP15H05686 to K.M.), the Japan Agency for Medical Research and Development (AMED to K.J.I.), the Japan Intractable Diseases Research Foundation (K.M.), the Senri Life Science Foundation Kishimoto grant (to K.M.), the Japan Prize Foundation (to K.M.), the Mochida Memorial Foundation (to K.M.), the National Institute for Physiological Science ("General Collaborative Project" to K.M. and M.T.), the Osaka University International Joint Research Promotion Program (to S.A.), the Japan Agency for Medical Research and Development (AMED) translational research network program seeds A (to K.M.) and the Japan Rheumatism Foundation (to K.M.).

Received: December 18, 2016

Revised: April 11, 2017

Accepted: May 25, 2017

Published: June 27, 2017

REFERENCES

- Abrahamsen, B., Zhao, J., Asante, C.O., Cendan, C.M., Marsh, S., Martinez-Barbera, J.P., Nassar, M.A., Dickenson, A.H., and Wood, J.N. (2008). The cell and molecular basis of mechanical, cold, and inflammatory pain. *Science* 321, 702–705.
- Arias, F., Mata-Essayag, S., Landaeta, M.E., Capriles, C.H., Pérez, C., Núñez, M.J., Carvajal, A., and Silva, M. (2004). *Candida albicans* osteomyelitis: case report and literature review. *Int. J. Infect. Dis.* 8, 307–314.
- Bautista, D.M., Jordt, S.E., Nikai, T., Tsuruda, P.R., Read, A.J., Poblete, J., Yamoah, E.N., Basbaum, A.I., and Julius, D. (2006). TRPA1 mediates the inflammatory actions of environmental irritants and proalgesic agents. *Cell* 124, 1269–1282.

- Butler, J., Fleming, P., and Webb, D. (2006). Congenital insensitivity to pain—review and report of a case with dental implications. *Oral Surg. Oral Med. Oral Pathol. Oral Radiol. Endod.* *101*, 58–62.
- Caterina, M.J., Leffler, A., Malmberg, A.B., Martin, W.J., Trafton, J., Petersen-Zeit, K.R., Koltzenburg, M., Basbaum, A.I., and Julius, D. (2000). Impaired nociception and pain sensation in mice lacking the capsaicin receptor. *Science* *288*, 306–313.
- Chiu, I.M., Heesters, B.A., Ghasemlou, N., Von Hehn, C.A., Zhao, F., Tran, J., Wainger, B., Strominger, A., Muralidharan, S., Horswill, A.R., et al. (2013). Bacteria activate sensory neurons that modulate pain and inflammation. *Nature* *501*, 52–57.
- Ding, Y., Arai, M., Kondo, H., and Togari, A. (2010). Effects of capsaicin-induced sensory denervation on bone metabolism in adult rats. *Bone* *46*, 1591–1596.
- Gamaletsou, M.N., Kontoyiannis, D.P., Sipsas, N.V., Moriyama, B., Alexander, E., Roilides, E., Brause, B., and Walsh, T.J. (2012). *Candida* osteomyelitis: analysis of 207 pediatric and adult cases (1970–2011). *Clin. Infect. Dis.* *55*, 1338–1351.
- Gow, N.A.R., van de Veerdonk, F.L., Brown, A.J.P., and Netea, M.G. (2011). *Candida albicans* morphogenesis and host defence: discriminating invasion from colonization. *Nat. Rev. Microbiol.* *10*, 112–122.
- Hoshino, K., Takeuchi, O., Kawai, T., Sanjo, H., Ogawa, T., Takeda, Y., Takeda, K., and Akira, S. (1999). Cutting edge: Toll-like receptor 4 (TLR4)-deficient mice are hyporesponsive to lipopolysaccharide: evidence for TLR4 as the Lps gene product. *J. Immunol.* *162*, 3749–3752.
- Ishibashi, K., Miura, N.N., Adachi, Y., Ogura, N., Tamura, H., Tanaka, S., and Ohno, N. (2002). Relationship between the physical properties of *Candida albicans* cell wall beta-glucan and activation of leukocytes in vitro. *Int. Immunopharmacol.* *2*, 1109–1122.
- Julius, D. (2013). TRP channels and pain. *Annu. Rev. Cell Dev. Biol.* *29*, 355–384.
- Kashem, S.W., Riedl, M.S., Yao, C., Honda, C.N., Vulchanova, L., and Kaplan, D.H. (2015). Nociceptive sensory fibers drive interleukin-23 production from CD301b(+) dermal dendritic cells and drive protective cutaneous immunity. *Immunity* *43*, 515–526.
- Kim, T., Yoon, J., Cho, H., Lee, W.B., Kim, J., Song, Y.H., Kim, S.N., Yoon, J.H., Kim-Ha, J., and Kim, Y.J. (2005). Downregulation of lipopolysaccharide response in *Drosophila* by negative crosstalk between the AP1 and NF-kappaB signaling modules. *Nat. Immunol.* *6*, 211–218.
- Kullberg, B.J., and Arendrup, M.C. (2015). Invasive Candidiasis. *N. Engl. J. Med.* *373*, 1445–1456.
- Lionakis, M.S., and Netea, M.G. (2013). *Candida* and host determinants of susceptibility to invasive candidiasis. *PLoS Pathog.* *9*, e1003079.
- Luche, H., Weber, O., Nageswara Rao, T., Blum, C., and Fehling, H.J. (2007). Faithful activation of an extra-bright red fluorescent protein in “knock-in” Cre-reporter mice ideally suited for lineage tracing studies. *Eur. J. Immunol.* *37*, 43–53.
- Maruyama, K., Fukasaka, M., Vandenbon, A., Saitoh, T., Kawasaki, T., Kondo, T., Yokoyama, K.K., Kidoya, H., Takakura, N., Standley, D., et al. (2012a). The transcription factor Jdp2 controls bone homeostasis and antibacterial immunity by regulating osteoclast and neutrophil differentiation. *Immunity* *37*, 1024–1036.
- Maruyama, K., Kawagoe, T., Kondo, T., Akira, S., and Takeuchi, O. (2012b). TRAF family member-associated NF- κ B activator (TANK) is a negative regulator of osteoclastogenesis and bone formation. *J. Biol. Chem.* *287*, 29114–29124.
- Maruyama, K., Uematsu, S., Kondo, T., Takeuchi, O., Martino, M.M., Kawasaki, T., and Akira, S. (2013). Strawberry notch homologue 2 regulates osteoclast fusion by enhancing the expression of DC-STAMP. *J. Exp. Med.* *210*, 1947–1960.
- Maruyama, K., Fukasaka, M., Uematsu, S., Takeuchi, O., Kondo, T., Saitoh, T., Martino, M.M., and Akira, S. (2015). 5-Azacytidine-induced protein 2 (AZI2) regulates bone mass by fine-tuning osteoclast survival. *J. Biol. Chem.* *290*, 9377–9386.
- Miller, D.J., and Mejicano, G.C. (2001). Vertebral osteomyelitis due to *Candida* species: case report and literature review. *Clin. Infect. Dis.* *33*, 523–530.
- Nong, Y.H., Titus, R.G., Ribeiro, J.M.C., and Remold, H.G. (1989). Peptides encoded by the calcitonin gene inhibit macrophage function. *J. Immunol.* *143*, 45–49.
- Pfaller, M.A., and Diekema, D.J. (2004). Rare and emerging opportunistic fungal pathogens: concern for resistance beyond *Candida albicans* and *Aspergillus fumigatus*. *J. Clin. Microbiol.* *42*, 4419–4431.
- Rodríguez, D., Pigrau, C., Almirante, B., Gasser, I., Ruiz, I., and Pahissa, A. (2003). [Vertebral osteomyelitis due to *Candida* spp]. *Enferm. Infecc. Microbiol. Clin.* *21*, 568–570.
- Ruefli-Brasse, A.A., French, D.M., and Dixit, V.M. (2003). Regulation of NF-kappaB-dependent lymphocyte activation and development by paracaspase. *Science* *302*, 1581–1584.
- Saijo, S., Fujikado, N., Furuta, T., Chung, S.H., Kotaki, H., Seki, K., Sudo, K., Akira, S., Adachi, Y., Ohno, N., et al. (2007). Dectin-1 is required for host defense against *Pneumocystis carinii* but not against *Candida albicans*. *Nat. Immunol.* *8*, 39–46.
- Shimada, S.G., and LaMotte, R.H. (2008). Behavioral differentiation between itch and pain in mouse. *Pain* *139*, 681–687.
- Swanson, A.G. (1963). Congenital insensitivity to pain with anhidrosis. A unique syndrome in two male siblings. *Arch. Neurol.* *8*, 299–306.
- Underhill, D.M., and Iliev, I.D. (2014). The mycobiota: interactions between commensal fungi and the host immune system. *Nat. Rev. Immunol.* *14*, 405–416.
- Woolf, C.J., and Costigan, M. (1999). Transcriptional and posttranslational plasticity and the generation of inflammatory pain. *Proc. Natl. Acad. Sci. USA* *96*, 7723–7730.
- Xue, L., Morris, S.W., Orihuela, C., Tuomanen, E., Cui, X., Wen, R., and Wang, D. (2003). Defective development and function of follicular, marginal zone and B1 B cells. *Nat. Immunol.* *4*, 857–865.
- Yapar, N. (2014). Epidemiology and risk factors for invasive candidiasis. *Ther. Clin. Risk Manag.* *10*, 95–105.
- Zhang, Y., and Haga, N. (2014). Skeletal complications in congenital insensitivity to pain with anhidrosis: a case series of 14 patients and review of articles published in Japanese. *J. Orthop. Sci.* *19*, 827–831.
- Zimmermann, K., Leffler, A., Babes, A., Cendan, C.M., Carr, R.W., Kobayashi, J., Nau, C., Wood, J.N., and Reeh, P.W. (2007). Sensory neuron sodium channel Nav1.8 is essential for pain at low temperatures. *Nature* *447*, 855–858.

Cell Reports, Volume 19

Supplemental Information

**Nociceptors Boost the Resolution
of Fungal Osteoinflammation via
the TRP Channel-CGRP-Jdp2 Axis**

Kenta Maruyama, Yasunori Takayama, Takeshi Kondo, Ken-ichi Ishibashi, Bikash Ranjan Sahoo, Hisashi Kanemaru, Yutaro Kumagai, Mikaël M. Martino, Hiroki Tanaka, Naohito Ohno, Yoichiro Iwakura, Naoki Takemura, Makoto Tominaga, and Shizuo Akira

Supplemental Information

Nociceptors Boost the Resolution of Fungal Osteo-inflammation via the TRP channel-CGRP-Jdp2 axis

Authors:

Kenta Maruyama, Yasunori Takayama, Takeshi Kondo, Ken-ichi Ishibashi, Bikash Ranjan Sahoo, Hisashi Kanemaru, Yutaro Kumagai, Mikaël M. Martino, Kouji Kobiyama, Ken J. Ishii, Hiroki Tanaka, Naohito Ohno, Yoichiro Iwakura, Naoki Takemura, Makoto Tominaga, and Shizuo Akira

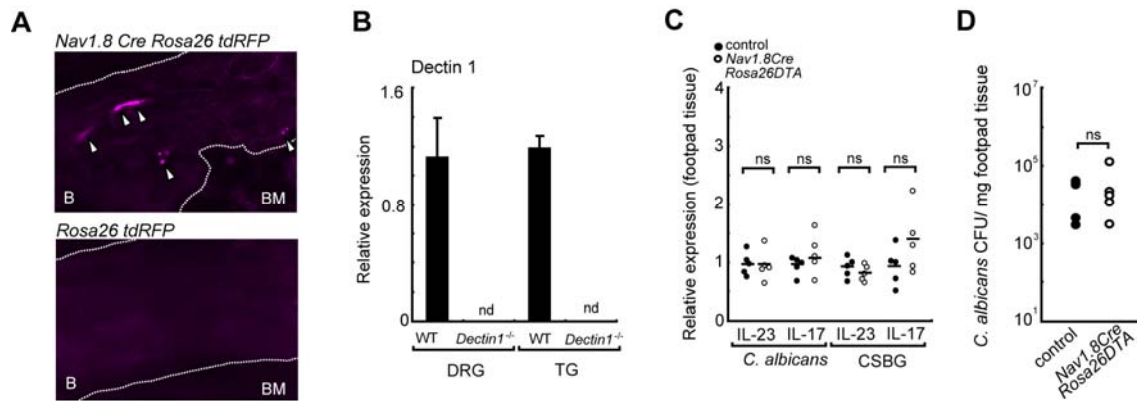


Figure S1. IL-23/IL-17 mediated fungal immunity is unaltered in Nav1.8-positive nociceptor

ablation, related to Figure 2. (A) A calcaneus bone section from *Nav1.8CreRosa26 tdRFP* mice was analyzed by fluorescent microscopy. Arrowheads indicate RFP-positive nociceptors. BM, bone marrow; B, bone. (B) Dectin-1 expression in DRG and trigeminal ganglions (TG). (C) *C. albicans* or CSBG were injected into the hind paws of *Nav1.8CreRosa26DTA* mice. After 6 days, IL-23 and IL-17 expression levels in hind paw tissues were measured by qPCR (n=5). (D) *C. albicans* was injected into the hind paws of *Nav1.8CreRosa26DTA* mice. After 6 days, the fungal burden of the footpad tissue was quantified (n=5). Error bars, S.E.; ns; not significant

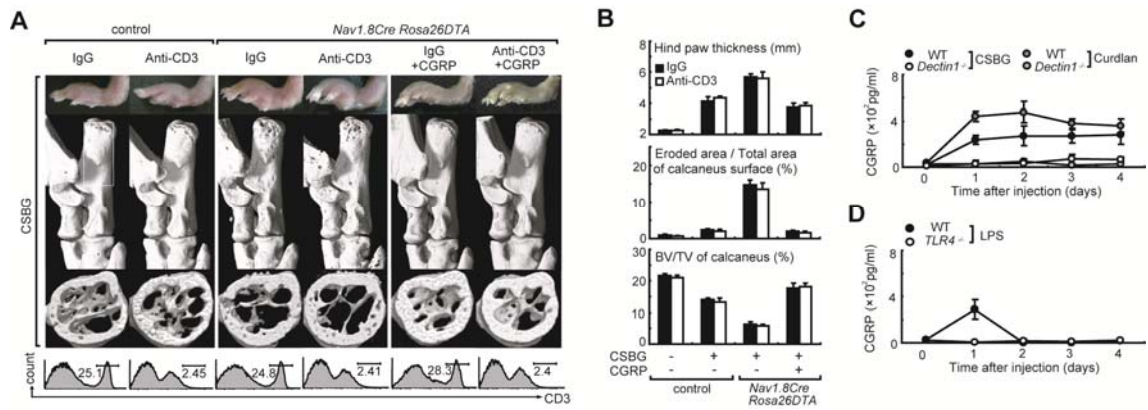


Figure S2. Dectin-1-mediated osteo-inflammation is potently suppressed by Nav1.8-positive nociceptor-derived CGRP, related to Figure 3. (A, B) To deplete T cells, anti-CD3 antibody (200 μ g/head, 17A2, eBioscience, United States) or isotype control antibody were intraperitoneally injected. After 12 h, CSBG was injected into the hind paws. Representative images of hind paws (upper), ankle μ CT images (middle), axial view of calcaneus μ CT images (lower), and splenic CD3-positive cell counts (bottom) at day 6 after CSBG injection are presented (A). Hind paw thickness, eroded area/total area of the calcaneus surface (%), and BV/TV of the calcaneus in (A) are indicated (B, n=5). (C) CSBG or curdlan (150 μ g) was injected into the hind paws of *Dectin-1*^{-/-} or WT mice and CGRP serum levels were measured (n=3). (D) LPS (150 μ g) was injected into the hind paws of *TLR4*^{-/-} or WT mice and CGRP serum levels were measured (n=3). Error bars, S.E.; * $p < 0.05$; ** $p < 0.01$; *** $p < 0.001$.

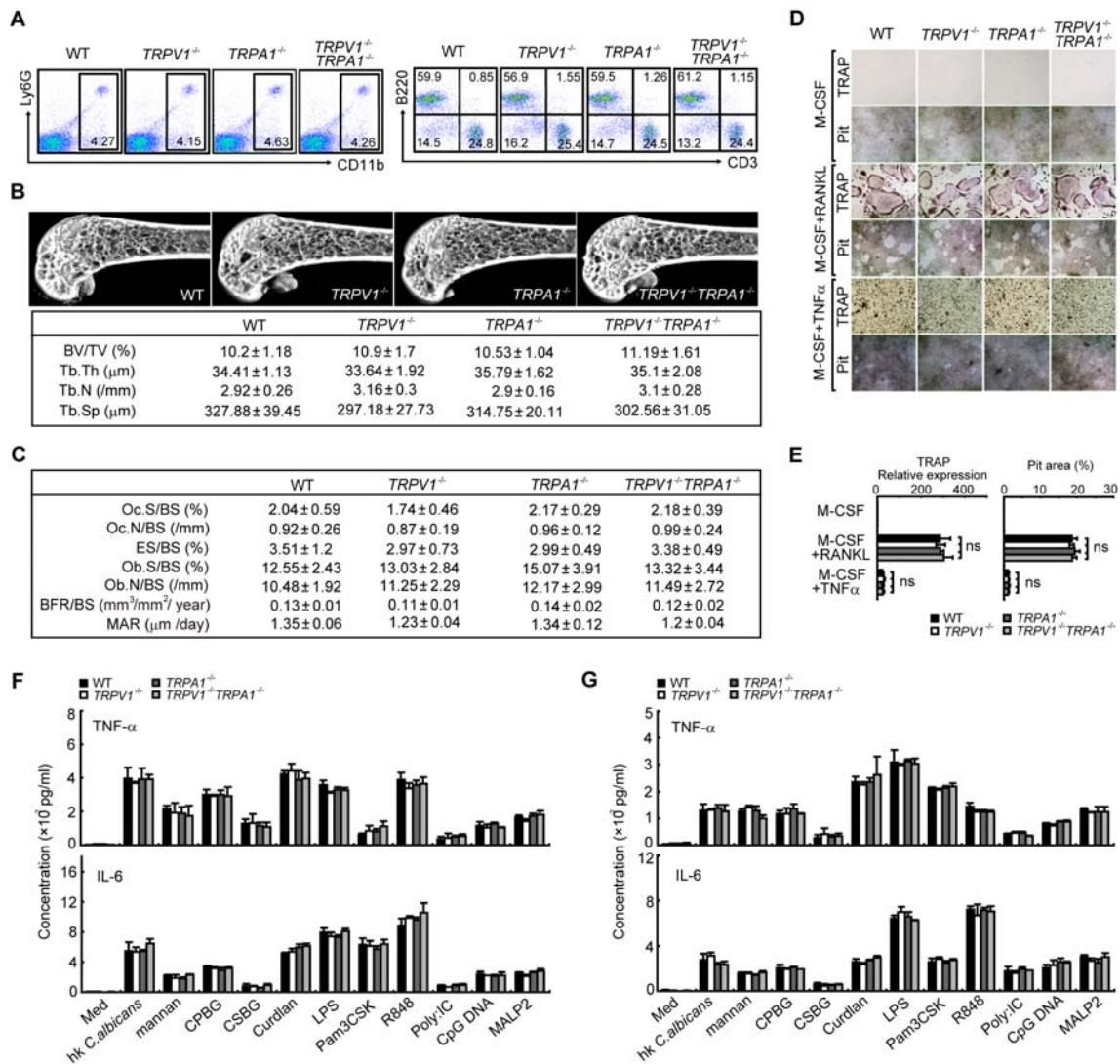


Figure S3. Bone metabolism, *in vitro* osteoclastogenesis, and *in vitro* myeloid cell cytokine production in TRPV1/TRPA1 deficiency, related to Figure 5. (A–C) Splenocytes from WT, *TRPV1*^{-/-}, *TRPA1*^{-/-}, and *TRPV1*^{-/-}*TRPA1*^{-/-} mice were analyzed by FACS (A). Representative μ CT images and bone morphometric analysis of distal femurs by μ CT (B). Bone histomorphometric analysis of the metaphyseal portion of tibias (C, n=7). (D, E) MDMs from WT mice, *TRPV1*^{-/-}, *TRPA1*^{-/-}, and *TRPV1*^{-/-}*TRPA1*^{-/-} mice were treated with RANKL or TNF- α . Representative TRAP staining and pit formation are indicated (D). TRAP expression levels (n=3) and pit area (%), n=6) were quantified (E). (F, G) MDMs (F) or neutrophils (G) from WT mice, *TRPV1*^{-/-}, *TRPA1*^{-/-} and *TRPV1*^{-/-}*TRPA1*^{-/-} mice were stimulated by various fungal and bacterial components for 24 h and TNF- α and IL-6 levels in the supernatants were measured (n=3). BV/TV, bone volume per tissue volume; Tb.Th, trabecular bone

thickness; Tb.N, trabecular bone number; Tb.Sp, trabecular bone spacing; Oc.S/BS, osteoclast surface per bone surface; Oc.N/BS, osteoclast number per bone surface; ES/BS, eroded surface per bone surface; Ob.S/BS, osteoblast surface per bone surface; Ob.N/BS, osteoblast number per bone surface; BFR/BS, bone formation rate per bone surface; MAR, mineral apposition rate; ns, not significant.

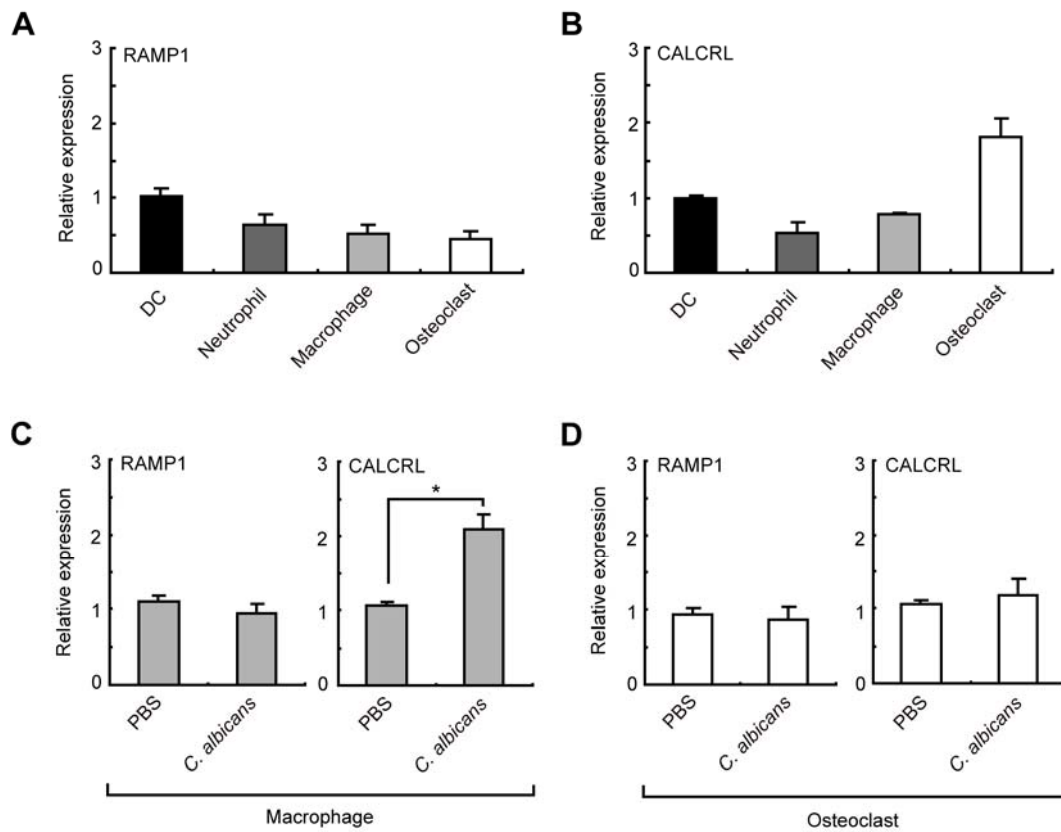


Figure S4. Expression of CGRP receptors in myeloid cells and osteoclasts, related to Figure 6. (A, B) RAMP1 (A) or CALCRL (B) expression levels in conventional dendritic cells (DC), neutrophils, MDMs (macrophages), and osteoclasts as quantified by qPCR (n=3). (C, D) MDMs (macrophages, C) and osteoclasts (D) were stimulated by live *C. albicans* or PBS for 3 h. Then, expression levels of RAMP1 (A) and CALCRL (B) were measured by qPCR (n=3). Error bars, S.E.; * $p < 0.05$.

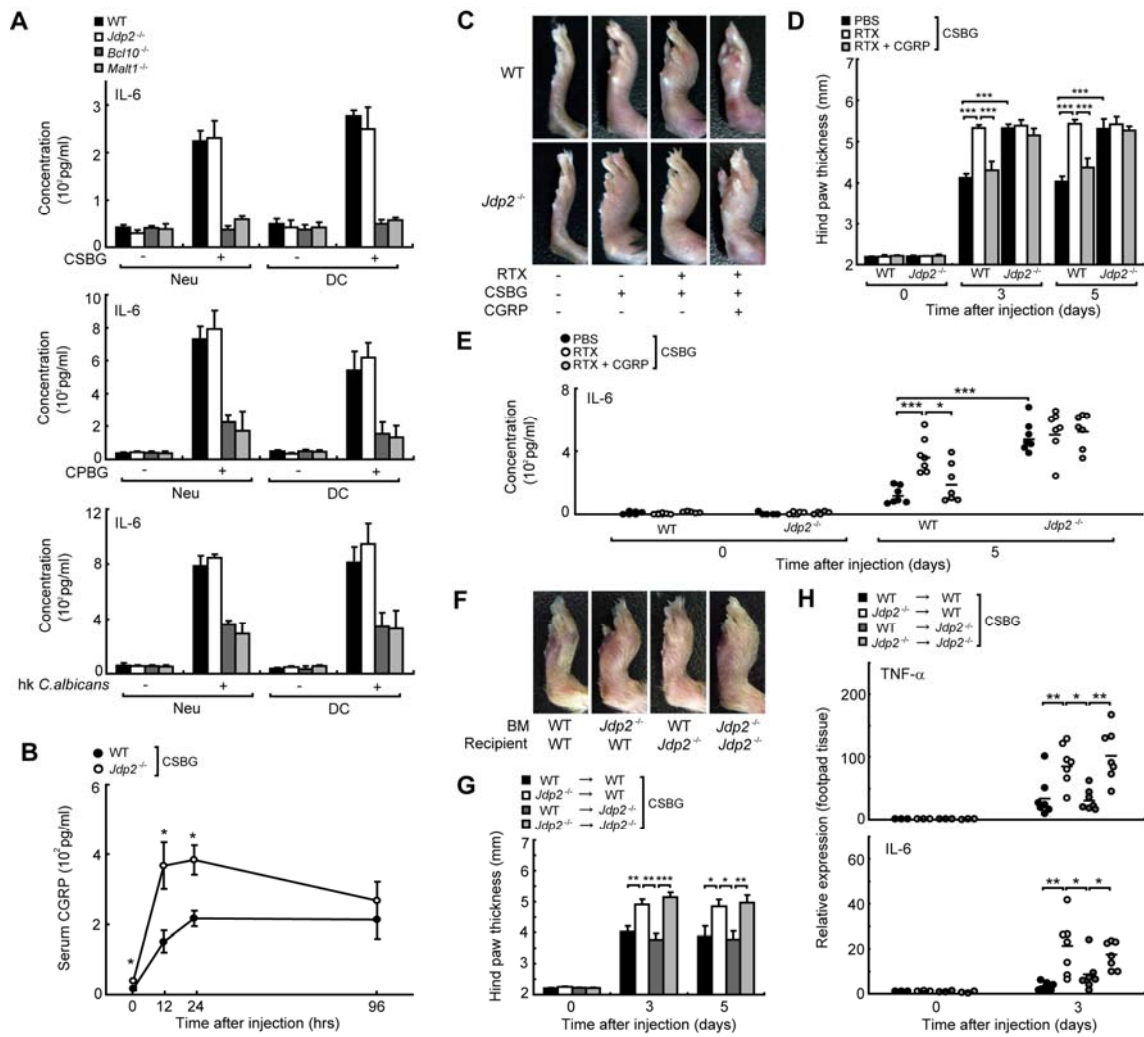


Figure S5. Characteristics of *Jdp2*-mediated immunosuppression by CGRP, related to Figure 7. (A) Neutrophils (Neu) or conventional dendritic cells (DC) from WT mice, *Jdp2*^{-/-} mice, *Bcl10*^{-/-} mice, and *Malt1*^{-/-} mice were stimulated by CSBG, CPBG, and hk *C. albicans*. After 24 h, supernatant IL-6 levels were measured (n=3). (B) CSBG was injected into the hind paws of *Jdp2*^{-/-} or WT mice and serum levels of CGRP were measured (n=4). (C–E) WT and *Jdp2*^{-/-} mice were treated with RTX as in Figure S4A. Then, CSBG and CGRP were injected into the hind paws. Representative images of hind paws at day 5 after injection are shown (C). Sequential hind paw thickness was measured (D). IL-6 serum concentrations were measured (E, n=7). (F–H) WT or *Jdp2*^{-/-} mice were irradiated and reconstituted with bone marrow from WT or *Jdp2*^{-/-} mice. After 7 weeks, CSBG was injected into the hind paws. Representative images of hind paws at day 5 after CSBG injection are presented (F). Sequential hind paw

thickness was measured (G). TNF- α and IL-6 expression in hind paws were measured by qPCR (H, n=7).

Error bars, S.E.; * $p < 0.05$; ** $p < 0.01$; *** $p < 0.001$.

Supplementary Methods

***C. albicans* preparation**

Yeast from fungal strains was cultured on potato dextrose agar plates (KOHJIN BIO, Saitama, Japan) at 30°C. After a 30-h incubation, cells were harvested from potato dextrose agar plates, suspended in PBS, and counted using a hemocytometer and trypan blue staining. To generate hk *C. albicans*, fungi were treated at 56°C for 30 min.

Preparation of pathogen-associated molecular patterns

C. albicans-derived purified mannan, designated mannan, was obtained from the National Institute for Biological Standards and Control (NIBSC code 76/515, non WHO reference material). *C.*

albicans-derived β -glucan was prepared as previously described (Ishibashi et al., 2002). Briefly, acetone-dried *C. albicans* NRBC1385 was suspended in 0.1 M NaOH with NaClO (final concentration, 1%) for 1 day at 4°C. After the reaction was completed, the reaction mixture was centrifuged and the particulate fraction was collected and dried by ethanol and acetone. The dried particulate fraction was then suspended in saline and sonicated for 30 s. After centrifugation, the supernatant was removed and the particulate fraction was designated CPBG. To prepare CSBG, CPBG suspended in DMSO was ultrasonically disrupted and the resulting supernatant was designated as CSBG. Lipopolysaccharide (L9764, Sigma-Aldrich, United States), the Dectin-1 agonist curdlan (C7821, Sigma-Aldrich), poly(I:C) (Amersham Biosciences, Piscataway, NJ, USA) were purchased. MALP-2 was prepared as previously described (Takeuchi et al., 2001), R-848 was provided by the Pharmaceuticals and Biotechnology Laboratory of the Japan Energy Corporation (Toda, Saitama, Japan), and the CpG oligonucleotide and a synthetic *N*-palmitoyl-S-dipalmitoylglyceryl (Pam₃) Cys-Ser-(Lys)₄ (CSK4) were generated as described previously (Maruyama et al., 2012a).

Injection of pathogens and their components

Injection into the hind paws or cheeks was performed using a 30-gauge needle (Becton Dickinson). For fungal infection, 25 μ l of the live or hk yeast form of the fungi in PBS was injected subcutaneously into the hind paws. CSBG (150 μ g) was also subcutaneously injected into the hind paws of mice. In some experiments, CSBG was injected with or without CGRP (1 μ M, 25 μ l, C0167, Sigma Aldrich) into the hind paws. After CSBG injection, blood samples were sequentially collected for the quantification of

cytokine or neuropeptide levels and calcaneus were radiologically analyzed.

In vivo antibody injection

To deplete T cells, anti-CD3 antibody (200 µg/head, 17A2, eBioscience, United States) or isotype control antibody were intraperitoneally injected at 12 h before CSBG injection into the hind paws of mice. To neutralize TNF- α , anti-TNF- α antibody (200 µg/head, TN3-19.12, BioLegend, United States) or isotype control antibody were intraperitoneally injected at 12 h before CSBG injection into the hind paws. For paw thickness evaluation, a digital micrometer (CD67-S PM, Mitutoyo, Kanagawa, Japan) was used.

DRG neuron isolation

Adult WT and *Dectin-1*^{-/-} male mice (10 to 12 weeks) were anesthetized by isoflurane. The DRGs were separated from L1–L6 in mice after perfusion with 10 mL ice-cold artificial cerebrospinal fluid (aCSF; 124 mM NaCl, 5 mM KCl, 1.2 mM KH₂PO₄, 1.3 mM MgSO₄, 2.4 mM CaCl₂, 10 mM glucose, 24 mM NaHCO₃, equilibrated with 95% O₂ and 5% CO₂ for 1 h on ice). The tissues were incubated with 725 µg collagenase type IX (lot# SLBG3258V and SLBG3259V, Sigma-Aldrich) in 250 µL Earle's balanced salt solution (Sigma-Aldrich) at 37°C for 25 min. Next, DRG neurons were mechanically separated by 10–20 cycles of pipetting using a small diameter Pasteur pipette. The neurons were centrifuged three times at 300 × g for 5 min at 4°C. Then, the supernatants were discarded and fresh PBS or aCSF was added to wash out the collagenase. The isolated neurons were placed on 12-mm-diameter coverslips (Matsunami, Japan) with 40 µl of aCSF and maintained at room temperature in a 95% O₂ and 5% CO₂ humidified chamber. The DRG neurons were used for experiments between 2 and 6 h after isolation.

Cells, tissues, and reagents

Antibodies for FACS analysis were purchased from BD Biosciences, and cells were stained with the indicated antibodies. Data were acquired using FACSCalibur (BD Biosciences), and analyzed by FlowJo software (Ashland, OR, USA). Neutrophils were harvested from the peritoneal cavities of mice after intra-peritoneal injection of thioglycollate as described previously (Maruyama et al., 2012a). MDMs and conventional dendritic cells were prepared as previously described (Fukasaka et al., 2013; Maruyama et al., 2012a). Neutrophils, MDMs, and dendritic cells were harvested, washed with PBS, and then placed into a 96-well tissue culture plate containing hk *C. albicans*, mannan, CPBG, or CSBG (α -MEM supplemented with non-inactivated 10% FCS) to test cytokine production. To generate osteoclasts, MDMs were cultured in the presence of 25 ng/ml M-CSF plus 75 ng/ml RANKL (R&D, Minneapolis,

United States) or 25 ng/ml M-CSF plus 75 ng/ml TNF- α (315-01A, Peprotech, United States) for 4–5 days. TRAP staining and F-actin staining was performed as described previously (Maruyama et al., 2012a). For the pit assay, osteoclasts were cultured on dentine slices (Wako Chemical, Osaka, Japan) or bone resorption assay plates (BRA-48P, PG research, Tokyo, Japan). After 5 days, plates were immersed for 3 h in 1 M NH₄OH, and resorption pits were observed by scanning electron microscopy (SEM; Hitachi MiniScope TM-1000). Cell death was quantified by a Cell Death Detection ELISA (1544675, Roche, Swiss). In some experiments, cAMP levels in MDMs or osteoclasts were measured using a cAMP Biotrak EIA system (RPN2251, GE Healthcare, United Kingdom). Synovial fluids and tissues were collected from the ankle joint of *C. albicans*-infected mice by flushing of the open joint cavity with 20 μ l of PBS. After flushing, synovial tissues were placed into the PBS and homogenized using a Biomasher (Nippi). Recombinant neuropeptides such as CGRP (C0167, Sigma-Aldrich, United States), Neurokinin A (N4267, Sigma Aldrich), Galanin (G0278, Sigma Aldrich, United States), Substance P (4014-V, Peptide Institute, Osaka, Japan), and Somatostatin (S1763, Sigma, United States) were used in these experiments, as well as 8-bromoadenosine 3,5'-cyclic monophosphate sodium salt (B7880, Sigma, United States), designated as cAMP.

Protein analysis

Western blotting was performed as previously described (Maruyama et al., 2012b). Proteins were detected using anti-Jdp2 (Weidenfeld-Baranboim et al., 2009), anti-NF- κ B-p65 (C-20; Santa Cruz Biotechnology), and anti-actin (C-11, Santa Cruz Biotechnology). For immunoprecipitation, pre-cleared cell lysates were incubated with protein A-sepharose (GE Healthcare) containing anti-Jdp2 antibodies or control IgG (Y-11; Santa Cruz Biotechnology) for 1 h at 4°C. The immunoprecipitants were washed, eluted, and then analyzed by western blotting.

Chromatin immunoprecipitation

To perform chromatin immunoprecipitation, cells were fixed with 5% formaldehyde, washed using PBS containing complete mini, and then resuspended in lysis buffer (1% SDS, 10 mM EDTA, 50 mM Tris-HCl, pH 8.1). After harvesting the cells, sonication (S220, Covaris, Woburn, MA, USA) was performed to obtain the DNA fragments. Antibodies against anti-NF- κ B-p65 (C-20; Santa Cruz Biotechnology) were pre-incubated overnight with 60 μ l of Dynabeads in PBS. Beads were then added to lysates and incubation was allowed to proceed overnight. Beads were washed once with High Salt

Immune Complex Wash Buffer (Millipore), once with Low Salt Immune Complex Wash Buffer (Millipore), seven times using LiCl Immune Complex Wash Buffer (Millipore), and finally with TE containing 50 mM NaCl. DNA was eluted in elution buffer (1% SDS 10 mM EDTA, 50 mM Tris-HCl, pH 8.1) and cross links reversed by incubation overnight at 65°C. After RNase A and proteinase K treatment, DNA was purified via ethanol precipitation using Etachinmate (Nippon Gene Ltd., Tokyo, Japan). DNA (200 ng) was used for the fragment library. Precipitated DNA was analyzed by PCR using primers that detect sequences containing the NF- κ B binding site of the TNF- α promoter (5'-GCCACTTCCTCCAAGAACT-3' and 5'-TTGGAAAGTTGGGGACACC-3') and the NFATc1 promoter (5'-CCGGGACGCCCATGCAATCTGTAGTAATT-3' and 5'-GCGGGTGCCCTGAGAAAGCTACTCTCCCTT-3').

Viral gene transfer

Jdp2 and NF- κ B p65 were cloned into the pCMV-SPORT6 vector. Jdp2 was also cloned into the retroviral vector pLZR-IRES/GFP (Kawagoe et al., 2009). Retroviral packaging was performed using PlatE. Viral gene transduction into MDMs was performed as previously described (Maruyama et al., 2012a). After transduction, MDMs were resuspended in 25 ng/ml M-CSF-supplemented medium (α -MEM containing 10% FCS). After 3 days, cells were harvested and replated onto CSBG- or CPBG-containing tissue culture plates. In some experiments, cells were further stimulated with 50 ng/ml RANKL.

Radiological and histological analysis of bone

To measure bone formation, double calcein labeling was performed. We intraperitoneally injected calcein (Wako, 16 mg/kg body weight) into mice and repeated the dose 72 h later. The mice were euthanized 24 h after the second injection, and their femurs were fixed with 70% ethanol before being subjected to morphometric analysis. Three-dimensional μ CT analysis of femurs and ankle joints was conducted using a Scan-Xmate RB080SS110 system (Comscan Techno Co., Ltd., Sagamihara, Japan). Bone structural indices were measured using TRI/3D-Bon software (Ratoc System Engineering Co., Ltd., Tokyo, Japan). Bone micro-architectural parameters were analyzed in the trabecular regions of femurs (from 0.1 to 1.5 mm away from the chondro-osseous junction) and calcaneus (from 0.1–1 mm away from the calcaneal tuberosity). To quantify the lateral surface calcaneus erosion, 3D images (1 \times 2 mm) were used to calculate the proportion of the calcaneus surface erosion area. The total area of bone erosion in the 1 \times 2 mm lateral surface calcaneus images was measured as pixels with ImageJ software and divided by the

total number of pixels. For histomorphometric analysis, tibias were fixed with 70% ethanol, stained with Villanueva Bone Stain (Wako, Tokyo, Japan), and then embedded in MMA. Serial longitudinal sections (6-mm thickness) were prepared using a microtome RM2255 (Leica), and then analyzed using a Histometry RT Camera (System Supply Co., Ltd., Nagano, Japan). Bone morphometric parameters were defined as previously described (Maruyama et al., 2012a). In some experiments, fixed calcaneus from *Nav1.8CreRosa26-tdRFP* mice were embedded in Tissue-tek OCT compound (Sakura) and frozen in -80°C. Frozen sections (of 8µm) were prepared using Cryostat (Leica CM1850) and Cryofilm and were analyzed fluorescent microscopy (BIOREVO BZ-9000, Keyence).

Supplementary References

- Fukasaka, M., Ori, D., Kawagoe, T., Uematsu, S., Maruyama, K., Okazaki, T., Kozaki, T., Imamura, T., Tartey, S., Mino, T., *et al.* (2013). Critical Role of AZI2 in GM-CSF-Induced Dendritic Cell Differentiation. *Journal of Immunology* *190*, 5702-5711.
- Ishibashi, K., Miura, N.N., Adachi, Y., Ogura, N., Tamura, H., Tanaka, S., and Ohno, N. (2002). Relationship between the physical properties of *Candida albicans* cell wall beta-glucan and activation of leukocytes in vitro. *International Immunopharmacology* *2*, 1109-1122.
- Kawagoe, T., Takeuchi, O., Takabatake, Y., Kato, H., Isaka, Y., Tsujimura, T., and Akira, S. (2009). TANK is a negative regulator of Toll-like receptor signaling and is critical for the prevention of autoimmune nephritis. *Nature Immunology* *10*, 965-U953.
- Maruyama, K., Fukasaka, M., Vandenbon, A., Saitoh, T., Kawasaki, T., Kondo, T., Yokoyama, K.K., Kidoya, H., Takakura, N., Standley, D., *et al.* (2012a). The Transcription Factor Jdp2 Controls Bone Homeostasis and Antibacterial Immunity by Regulating Osteoclast and Neutrophil Differentiation. *Immunity* *37*, 1024-1036.
- Maruyama, K., Kawagoe, T., Kondo, T., Akira, S., and Takeuchi, O. (2012b). TRAF Family Member-associated NF-kappa B Activator (TANK) Is a Negative Regulator of Osteoclastogenesis and Bone Formation. *Journal of Biological Chemistry* *287*, 29114-29124.
- Takeuchi, O., Kawai, T., Muhlrardt, P.F., Morr, M., Radolf, J.D., Zychlinsky, A., Takeda, K., and Akira, S. (2001). Discrimination of bacterial lipoproteins by Toll-like receptor 6. *International Immunology* *13*, 933-940.